Acta Astronautica 211 (2023) 631–649

Contents lists available at ScienceDirect

Acta Astronautica

journal homepage: www.elsevier.com/locate/actaastro

Research paper

Conditions at the interface between the space elevator tether and its climber

Dennis H. Wright [a,*], Larry Bartoszek [b], A.J. Burke [c], David Dotson [d], Hassan El Chab [e], John Knapman [f], Martin Lades [g], Adrian Nixon [f], Paul W. Phister Jr. [h], Peter Robinson [f]

[a] International Space Elevator Consortium (ISEC), USA
[b] Bartoszek Engineering, USA
[c] Institute of Electrical and Electronics Engineers (IEEE), USA
[d] ISEC, USA
[e] Jawharat Al Muhsen Group, Iraq
[f] ISEC, UK
[g] ISEC, Germany
[h] MANIAC Consulting, USA

ARTICLE INFO

Keywords:
Space elevator
Tethers
Graphene
Material properties

ABSTRACT

A simple space elevator consists of a single tether extending well beyond geosynchronous altitude and a payload-carrying device which grips and climbs the tether. A friction-based, opposing wheel climber was judged most likely to be constructed with present-day technology and it appears that mass-production of the tether material is also within reach. The physical conditions at the interface between the climber wheels and tether determine first of all the possibility of climbing and then the design parameters of the tether. Conditions such as lifting torque, tensile, compressive and shear strength, friction, interface temperature, thermal conductivity and radiative cooling were examined and used to set minimum requirements for the tether material. Graphene superlaminate (GSL), consisting of layers of single crystal graphene, appears to be an excellent tether material with a sufficiently high tensile strength. An increase in its inter-layer cross-bonding and a larger mutual coefficient of friction with the climber wheel material would allow it to satisfy the climbing conditions. A final determination of the suitability of GSL requires the measurement of a number of, as yet unknown, material properties. A list of such measurements is proposed and a partial list of trade studies and iterations of design for the tether are provided.

1. Introduction

The first effort to quantify the viability of an Earth-based space elevator in terms of the strength of its tether, the mass of its climber and the logistics of constructing and maintaining it, was the space elevator feasibility condition [1]. It assumed a simple space elevator concept [2], which is linearly scalable, to set limits on payload throughput, power requirements and the rate at which a space elevator could replace itself.

The primary inputs to the feasibility condition are the tensile strength and material density of the tether; the tether must be strong enough and light enough to support itself and any devices that climb it. Materials that satisfy this requirement, such as single crystal graphene (SCG) [3], hexagonal boron nitride (hBN) [4] and some varieties of carbon nanotubes [5] exist today in small quantities and it is expected that mass production of at least one of these will be seen in the near future [6]. An assessment of both tether and climber materials and their projected readiness for use was done by Swan et al. [7].

Aside from high strength and low density, many other requirements for the tether material remain unexamined. These can be identified and quantified by studying the way in which the space elevator climber interacts with the tether at the interface between the two. A climber must be able to grip the tether and propel itself up or down or remain stationary. This requirement can be referred to as "climbability", which consists of the set of conditions, such as friction, pressure, shear and heat transfer, which exist at the interface. A determination of the likely range of values for each of these parameters will allow an estimate of whether or not climbing is possible.

There are many proposals for climber drive mechanisms [8], varying mainly in the way in which they grip the tether. These include

* Corresponding author.
E-mail addresses: dennis.wright@isec.org (D.H. Wright), design@bartoszekeng.com (L. Bartoszek), ajburke@ieee.org (A.J. Burke), david.dotson@isec.org (D. Dotson), alchabhassan@gmail.com (H. El Chab), john.knapman@isec.org (J. Knapman), martin.lades@isec.org (M. Lades), adrian.nixon@isec.org (A. Nixon), phisterp@juno.com (P.W. Phister Jr.), peter.robinson@isec.org (P. Robinson).

https://doi.org/10.1016/j.actaastro.2023.06.047
Received 7 May 2023; Received in revised form 17 June 2023; Accepted 26 June 2023
Available online 28 June 2023
0094-5765/© 2023 The Authors. Published by Elsevier Ltd on behalf of IAA. This is an open access article under the CC BY license (http://creativecommons.org/licenses/by/4.0/).

Physical Constants

$\mu_E = 3.9860 \times 10^5$ km^3/s^2	Gravitational parameter of Earth
$g = 9.80665$ m/s^2	Standard gravity
$\Omega = 7.29212 \times 10^{-5}$ rad/s	Angular velocity of Earth
$R_E = 6378$ km	Equatorial radius of Earth
$R_G = 42164$ km	Geosynchronous orbit radius

Units

K	Kelvin
kg	kilogram
km	kilometers
N, kN, MN	Newton, kilo, mega
Pa, MPa, GPa, TPa	Pascal, mega, giga, tera
t	metric ton = 1000 kg
W, kW, MW	watt, kilo, mega

Acronyms

CNT	Carbon nanotube
GEO	Geostationary Earth orbit
GSL	Graphene super-laminate
hBN	Hexagonal boron nitride
LEO	Low Earth orbit
SCG	Single crystal graphene

Variable and Parameter Names

α_a, α_d	Angular acceleration, deceleration of wheel
κ	Electrical conductivity
λ	Thermal conductivity
μ	Coefficient of friction
ν	Poisson's ratio
ρ	Mass density
σ	Compressive or tensile stress
τ	Shear stress
ω	Angular velocity
A_c	Area of contact patch between wheel and tether
d	Radial deformation of wheel
E	Young's modulus
F_c	Compression force
F_t	Tractive force
f_{tav}	Ratio of trip-averaged clamp pressure to maximum clamp pressure
h	Altitude (distance above Earth's surface)
J	Rotational moment of inertia
M	Torque
m_c	Mass of climber
N_{wheels}	Number of climber wheels
N_{wp}	Number of wheel-pairs
P_L	Limiting mechanical power
R_{eff}	Effective wheel radius averaged over deformations
R_W	Undeformed wheel radius
S_f	Maximum fatigue stress
T	Temperature
v_{max}	Maximum climber velocity

electromagnetic, electrostatic and mechanical. Among the mechanical methods, friction-based drives appear to be the most efficient as well as being feasible with present-day technology. Once the tether and climber types are chosen, the set of conditions which apply at the interface can be developed and used to constrain the material properties of the tether.

1.1. Assumptions

In this study, it is assumed that a space elevator consists of a single tether, ascended by a single climber. The tether is 100,000 km long with a width of order one meter, varying with altitude. Each layer of SCG has a thickness of 0.335 nm so that 12,000 layers would give a total thickness of 4.1 μm. More layers would be required for a climber-bearing tether. Once the layers of SCG are optimally stacked, the tether material will become somewhat different: AB-stacked, single-crystal, multi-layer graphene, or graphene superlaminate (GSL) for short. While the density of SCG is 2260 kg/m^3 [9], the density of GSL will be slightly greater due to the stacking; it was calculated in this study to be 2298.5 kg/m^3.

It is likely that some combination of hBN and SCG will be used, and it is possible that advances in CNTs will make that the preferred material. For simplicity, though, pure GSL is assumed.

A length of 100,000 km is somewhat arbitrary. Without a counterweight at the apex of the space elevator, the tether length required to balance the forces would be longer. However, a station at the apex would be very useful and the greater its mass, the shorter the required length of the tether.

The climber has a mass of 20,000 kg (20 t), a value used in previous studies [2,10] and reasonable for the smaller, pilot tethers that are likely to be the first ones built. Taking into account deformations of the tether due to climbers [11], 20 t is appropriate for a combined tether and counterweight mass of around 2000 t. A much larger climber mass, of order 100,000 kg, is possible with more massive tethers and is certainly more desirable for its increased throughput. However, even with a pilot space elevator, 20 t would be a large improvement over rockets because of the greater frequency, regularity and safety of climber launches.

The climbing mechanism consists of opposing wheels which grip the tether. The wheels are driven by high-torque electric motors which can be built with present-day technology. It is further assumed that it takes about one week to ascend from the surface of the Earth to the altitude of geostationary orbit (GEO). Considering only the conditions at the climber–tether interface, effects due to the electromagnetic, radiation and chemical environment were judged to be small.

1.2. Choice of climber type

Several types of climber drive were considered [8] before settling on an opposed-wheel friction drive. A brief summary of these is presented here.

Magnetic levitation and related drives at first appeared ideal, with no tether contact and high speeds (on Earth) of 600 km/h [12]. However, large inefficiencies due to poor magnetic flux return make current designs a poor choice for space.

High voltages on conducting surfaces of two opposing climber wheels would generate large capacitive forces, pulling the nearby opposing surfaces closer together, in turn causing wheel rotation and thus lift. This electrostatic drive [8] has the potential to be quite fast but problems with large leakage currents need to be worked out.

A capstan drive, in which the tether is threaded through a set of staggered wheels, generates more than enough friction because of its large tether contact area. Compared to the opposed-wheel drive, however, more compressive force must be applied to the wheels both horizontally and vertically in order to keep the wheel axles in place.

Another possible problem is that the tether material may be brittle and intolerant of much bending.

Tank treads were proposed by Edwards [2] in his climber design. While this type of drive provides a large contact area with the tether, vertical operation is problematic. Gravity no longer holds the treads in contact, so that many bogey wheels must be added to compensate. With a sufficient number of extra wheels to provide contact, the tread itself is no longer useful and adds unnecessary weight. Treaded vehicles on Earth can reach speeds of up to 70 km/h [13].

In the end, an opposed-wheel friction drive appeared to be simplest and most efficient. This type of drive is used in some aerial trams which can achieve speeds of 45 km/h. Given its similarity in design to tank-tread drives and its much lower mass, such a drive should be at least as fast and probably faster than tank-treads.

1.3. Derived requirements and proposals

From these assumptions the compressive, tensile and shear stresses at the interface are derived. These in turn determine the requirements on the tether material. Improvements in tether material manufacture are proposed which will allow the requirements to be met. As a result, the material can be strengthened and the coefficient of friction between the climber wheels and tether material can be increased.

Finally, two studies are proposed in order to inform the proposed improvements in the material. Computer simulations of one- and two-dimensional macro-molecules under conditions of physical stress and chemical modification will need to be performed. These will indicate whether methods for increasing strength and friction in SCG are feasible. Once produced, the new material will need to be subjected to a program of testing and measurement in order to both characterize it and validate its strength.

2. The climbability condition

2.1. Introduction

The primary function of a space elevator is to transport a payload between a planetary surface and space. Any climber carrying that payload must interact with the tether in order to ascend or descend. It must do so in a reasonable amount of time, while carrying an economically feasible payload and being durable enough to survive long travel times and distances. All of these requirements comprise a general condition referred to here as climbability.

The central issue is whether or not the climber can propel itself up or down. This is referred to as local climbability, so-called because it deals with the immediate vicinity in which the climber grips the tether and because it concerns only the physical parameters making climbing possible. Issues such as climber velocity, power availability or payload are not considered in this case.

The interactions at the interface between the tether and the climber traction device must be identified so that local climbability conditions can be quantitatively defined. If the initial climber design satisfies these conditions, the broader issues of power and velocity optimization, payload mass throughput and maintenance may be considered.

Defining the local climbability conditions requires understanding of properties in four main areas:

- **performance parameters**, including design-independent parameters such as speed, mass and power consumption,
- **tether**, including material composition, maximum stress and maximum pressure,
- **climber**, encompassing drive type, wheel radius, available torque and scaling laws, and
- **climber–tether interface**, encompassing coefficient of friction, maximum interface pressure, tractive force and thermal behavior.

A reference compendium of the current understanding is collected in the Appendix. These data reflect the current consensus in material parameters. At the time of this study, the tether material is not available in sufficiently large quantities for practical testing. Thus, some of its properties are based on anticipated or extrapolated values. Section 3 discusses existing candidate materials, their properties and the prospects for adapting them to space elevator use.

The properties of materials and their interactions can be categorized as mechanical, electromagnetic, chemical, thermal and optical/radiative. For a friction drive, in this first assessment, electromagnetic, chemical and radiative aspects are not considered, although they are useful for the investigation of the details of friction, radiation damage and cross-bonding of tether layers, to name a few. The influence of those three, or the cross influence of all five properties, on the ultimate tether strength can be highly complex and is left for future investigation. This leaves mechanical and thermal interactions to be considered as the primary properties for the friction drive.

Ideally, material properties and interactions would be fully parameterized and the optimal traction for a given tether/climber configuration could be determined with a simple formula for climbability. This would permit easy substitutions as engineering progresses. However, due to the complexity of the interactions, some parameters are best captured by using reference designs of the climber. Reference designs can be tested with today's materials, allowing the resulting performance parameters to be extrapolated into the ranges which apply to a space elevator.

The description of the climber–tether interface begins with the basic mechanical properties in vacuum, which are applicable to most of the elevator, and can demonstrate how a climber holds position, accelerates and climbs. Once a basic set of parameters is established, it can be extended later with more complex and higher-order effects. These include force distributions imposed by realistic climber designs and other modalities such as heating due to friction or external sources such as sunlight, chemical changes in the tether, high energy radiation interacting with materials, electromagnetic fields interacting with climber and tether, and atmospheric effects such as wind, corrosion or lightning. All of these require further assessments.

2.2. Local climbability

Regardless of the type of drive it uses, a climber can be viewed as a black box which produces a tension differential in the tether between its entry and exit points. Between the surface of the Earth and geosynchronous altitude, an ascending climber takes in high tension tether at its upper end and releases lower tension tether at its lower end. The difference of the tensions is the force that supports and accelerates the climber. How this difference is produced depends on the drive type. Opposing, counter-rotating climber wheels are clamped against one another in order to exert pressure on the tether. The mutual friction between wheels and tether supplies the tractive force required to move the climber. Each wheel is driven by a motor whose shaft is directly coupled to the axle without a gearbox or torque converter. It is assumed that the center of mass of the climber is located along the tether axis. This condition is met by supplying automated climber steering and adjustable clamping forces on the wheels.

Fig. 1 shows the essential part of an opposed-wheel friction drive: the tether and one of the two wheels which pinch it. As the wheel rotates, a tractive force F_t is generated from the compressive force F_c and the friction between the wheels and the tether. Electric motors provide the torque $M = R_W \times F_t$, where R_W is the wheel radius. The sum of tractive forces from multiple pairs of wheels increases the tension in the upper tether and decreases it in the lower tether so that $T_{up} - T_{down} = m_c[a(r) - g(r)]$, where m_c is the climber mass and $a(r)$ is

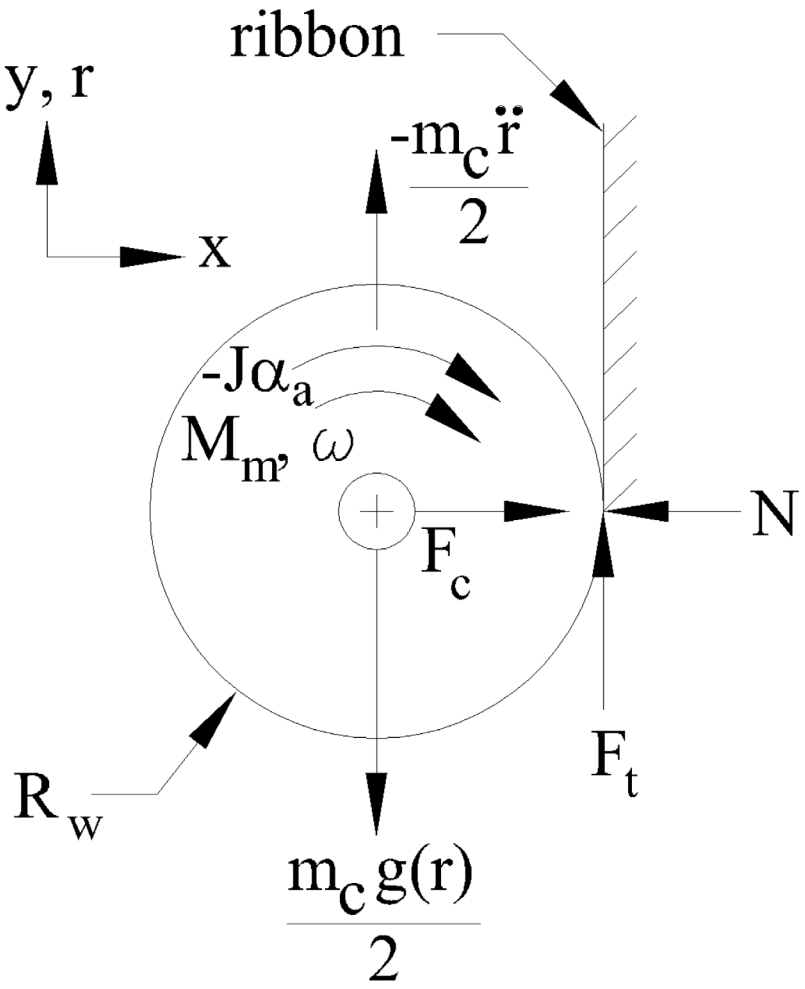

Fig. 1. Free body force diagram for one climber wheel in contact with the tether. The compressive force F_c is directed perpendicular to the tether (ribbon) so that a normal force N is created. The tractive force F_t is generated by motors providing a torque M_m across a wheel radius R_W. The total upward acceleration $\ddot{r}$ must overcome the effective gravitational acceleration $g(r)$. m_c is the climber mass. ω is the angular velocity and α the angular acceleration of the wheel. The factor $\frac{1}{2}$ in the upward and downward forces reflects the fact that only one of the two pinching wheels is shown in the force diagram.

the total acceleration as function of altitude which must overcome the effective gravity $g(r)$.

2.2.1. Performance parameters

A large number of parameters, some as yet unknown, will have to be specified in order to build a working climber. Some do not directly affect the mechanics of the climber–tether interface, but need to be set as a starting point in the design of the climber. These parameters have to do with climber performance and were chosen on the basis of economics and efficiency.

Climber Mass

The tether mass imposes an upper bound on the climber mass; it is therefore assumed that the tether mass is sufficiently large to support a 20,000 kg climber. Such a climber might consist of 6000 kg of climber mechanism and 14,000 kg of payload. These values are guesses which provide an economically attractive throughput to GEO [2], while allowing a sufficient mass budget for the climber mechanism.

This study deals with the effects of a single climber on the tether. In operational mode, the space elevator will have several climbers on the tether at any one time. How their total mass and departure frequency will affect the tether load and mass is taken into account elsewhere [14].

Time of Climb to GEO and Maximum Power

The desired transit time to GEO determines the velocity of the climber, the radius of the climber wheels and ultimately the stresses exerted on the tether. The velocity, and therefore the energy consumed by a climber as it travels from the surface of the Earth to GEO, is critical to the commercial viability of the space elevator. Reasonable values of the energy require that power and transit time be balanced against one another, with power in this case meaning mechanical power only. Due to motor inefficiencies, large at lift-off and small at most other times, total power expended is always greater than mechanical power.

One method of power management is to cap the mechanical power of the climber. This results in a distinct power profile in each of four time periods which comprise the transit time to GEO: initial acceleration from rest to maximum power (Δt_{ia}), constant maximum power (Δt_{cp}), gradual power reduction imposed by a constant climber speed limit (Δt_{cv}) and deceleration to rest at GEO (Δt_{dc}).

The period of constant maximum mechanical power lasts until a climber speed limit is reached. With constant power and decreasing effective gravity as a function of altitude, the velocity would increase

without limit. Practical considerations such as friction at the climber–tether interface, steering and the velocity-dependent Coriolis force make a speed limit necessary.

The total transit time, derived in [8], is

$$\Delta t = \Delta t_{ia} + \Delta t_{cp} + \Delta t_{cv} + \Delta t_{dc}\ , \tag{1}$$

or

$$\Delta t = \frac{P_L}{\alpha_a m_c \left[\mu_E/R_E^2 - \Omega^2 R_E\right]} + \frac{m_c}{P_L}\left[\mu_E\left(\frac{1}{R_E+h_1} - \frac{1}{R_E+h_2}\right) - \Omega^2\left(\frac{(R_E+h_2)^2-(R_E+h_1)^2}{2}\right)\right] + \frac{h_3-h_2}{v_{max}} + \frac{v_{max}}{R_W \alpha_d}. \tag{2}$$

The climber parameters here are P_L, the mechanical power limit, m_c, the mass, v_{max} the maximum allowed velocity and R_W, the climber wheel radius. α_a is the initial angular acceleration of the wheel and α_d is the final angular deceleration. R_E, Ω and μ_E are the Earth radius, angular velocity and gravitational parameter. h_1 is the altitude at which maximum mechanical power is reached, h_2 is the altitude at which the maximum velocity is reached and h_3 is the altitude at which deceleration to GEO begins.

The time to GEO thus depends on five climber parameters: the specific power P_L/m_c, v_{max}, R_W, α_a and α_d.

A past climber study [10] suggested that reasonable values of the limiting power and maximum velocity would be 4 MW and 200 km/h (55.56 m/s). A high-torque motor [15] could provide $M_m = 5600$ N-m at 1900 RPM and would drive a likely angular moment of inertia of $J = 5$ kg m^2. For a 20,000 kg climber with ten wheels, the climber mass per wheel, m_w, is 2000 kg. To achieve a velocity of 200 km/h at 1900 RPM requires a wheel radius $R_W = 0.2794$ m.

Now the initial angular acceleration α_a can be derived from Fig. 1 :

$$\alpha_a = \frac{M_{motor} - m_w R_W \left[\mu_E/R_E^2 - \Omega^2 R_E\right]}{J + m_w R_W^2}. \tag{3}$$

Using the above values yields

$$\alpha_a = \frac{5600 \text{ N-m} - (2000 \text{ kg})(9.8 \text{ m/s}^2)(0.2794 \text{ m})}{5 \text{ kg m}^2 + (2000 \text{ kg})(0.2794 \text{ m})^2} = 0.768 \text{ s}^{-2}.$$

At that initial acceleration, the time it takes to reach maximum mechanical power is

$$\Delta t_{ia} = \frac{P_L}{\alpha_a R_W m_c \left[\mu_E/R_E^2 - \Omega^2 R_E\right]}\ , \tag{4}$$

so that with a specific power $P_L/m_c = 200$ W/kg and the above value for the angular acceleration,

$$\Delta t_{ia} = \frac{200 \text{ W/kg}}{(0.768/\text{s}^2)(0.2794 \text{ m})(9.8 \text{ m/s}^2)} = 95.1 \text{ s}\ .$$

The velocity reached at that time follows:

$$v = R_W \alpha_a \Delta t_{ia} = 20.4 \text{ m/s} = 73.5 \text{ km/h}\ , \tag{5}$$

as does the altitude

$$h_1 = \frac{1}{2} R_W \alpha_a \Delta t_{ia}^2 = 0.5(0.768/\text{s}^2)(0.2794 \text{ m})(95.1 \text{ s})^2 = 970 \text{ m}. \tag{6}$$

With the above values of specific power and maximum velocity, $h_2 = 4064$ km. Using these values for h_1 and h_2, yields the total time at constant, limited power $\Delta t_{cp} = 120{,}660$ s = 33.52 h = 1.40 d.

The deceleration time is small even with small deceleration, so its value is somewhat arbitrary. Setting it to twice the initial acceleration, $\alpha_d = 1.536$ s^{-2}, so that the time it takes to stop is

$$\Delta t_{dc} = \frac{55.56 \text{ m/s}}{(0.2794 \text{ m})(1.536 \text{ s}^{-2})} = 129.5 \text{ s}\ .$$

The stopping distance is

$$0.5(1.536 \text{ s}^{-2})(0.2794 \text{ m})(129.5 \text{ s})^2 = 3596 \text{ m}$$

so that the altitude h_3 is

$$h_3 = R_G - R_E - 3.6 \text{ km} = 35{,}782.4 \text{ km}. \tag{7}$$

Finally, the total time at maximum velocity is

$$\Delta t_{cv} = \frac{h_3 - h_2}{v_{max}} = \frac{35782.4 \text{ km} - 4064 \text{ km}}{200 \text{ km/h}} = 570{,}931.2 \text{ s}\ . \tag{8}$$

The total travel time is thus 691,816 s = 192.17 h = 8.01 days. If a higher climber velocity were possible, for example 300 km/h, the specific power could be lowered to 150 W/kg, giving a total transit time of 6.51 d. A summary of altitude and time values for each power region is shown in Fig. 2.

Climber and Tether Environment

Parameters related to the robustness of materials against the electromagnetic, radiation and chemical surroundings are currently not available in detail for this study.

2.2.2. Climber–tether interface

Conditions at the interface between the climber wheel and tether can be understood in terms of the contact patch. Hertzian contact theory provides a way to calculate the stresses in this region, given the material parameters of wheel and tether, the coefficient of friction between them and the forces applied by the climber mechanism. The resulting interface stresses define the minimal material strengths required for climbing and allow estimates of heat build-up in the wheels and tether.

Friction

The key parameter in converting the compressive force supplied by the climber into tractive force is the coefficient of friction μ,

$$F_t = \mu F_c. \tag{9}$$

μ depends on the materials and surfaces of the two components in contact and is almost always an empirical parameter, rather than one that can be calculated. For most mechanical applications, the value of μ between two materials is well measured, but in the case of SCG it is not. Almost all measurements to date use atomic force microscopes with diamond-tipped probes, leading to values of μ more appropriate to SCG-carbon interfaces than to SCG-metal interfaces. A recent diamond-probe value of μ for SCG is 0.03 (Table A.1), in the lubricant range. Metal-tipped probes, when they become available, may return more applicable values, and these may be higher.

For practical applications, μ must be greater than 0.05, though 0.1 is much more common. If new data do not reveal a higher coefficient of friction, it is possible to modify GSL to increase it. Methods to do so are discussed in Section 3. In the calculations that follow, $\mu = 0.1$ is assumed to be the minimum value.

Temperature

The maximum temperature at the interface must not be greater than the lower of the maximum operating temperatures of the wheel or the tether,

$$T_{interface} \le min(T_{maxW}, T_{maxT}). \tag{10}$$

The melting temperature of SCG (5500 K, Appendix) is much higher than that of any likely wheel material. Titanium alloys, for example, melt at around 1900 K. This suggests that the maximum tether operating temperature will be much higher than that of the climber wheels. Thus, the wheel material determines the interface maximum, and wheel cooling must be considered.

Pressure

The area of contact between the drive wheel and the tether, and the pressure there, can be calculated by Hertzian contact theory [16]. For a cylinder pressed against a plane, or tether in this case, the pressure varies along the width of the tether as

$$P(x) = P_{max}\sqrt{1 - \frac{a^2}{x^2}} \tag{11}$$

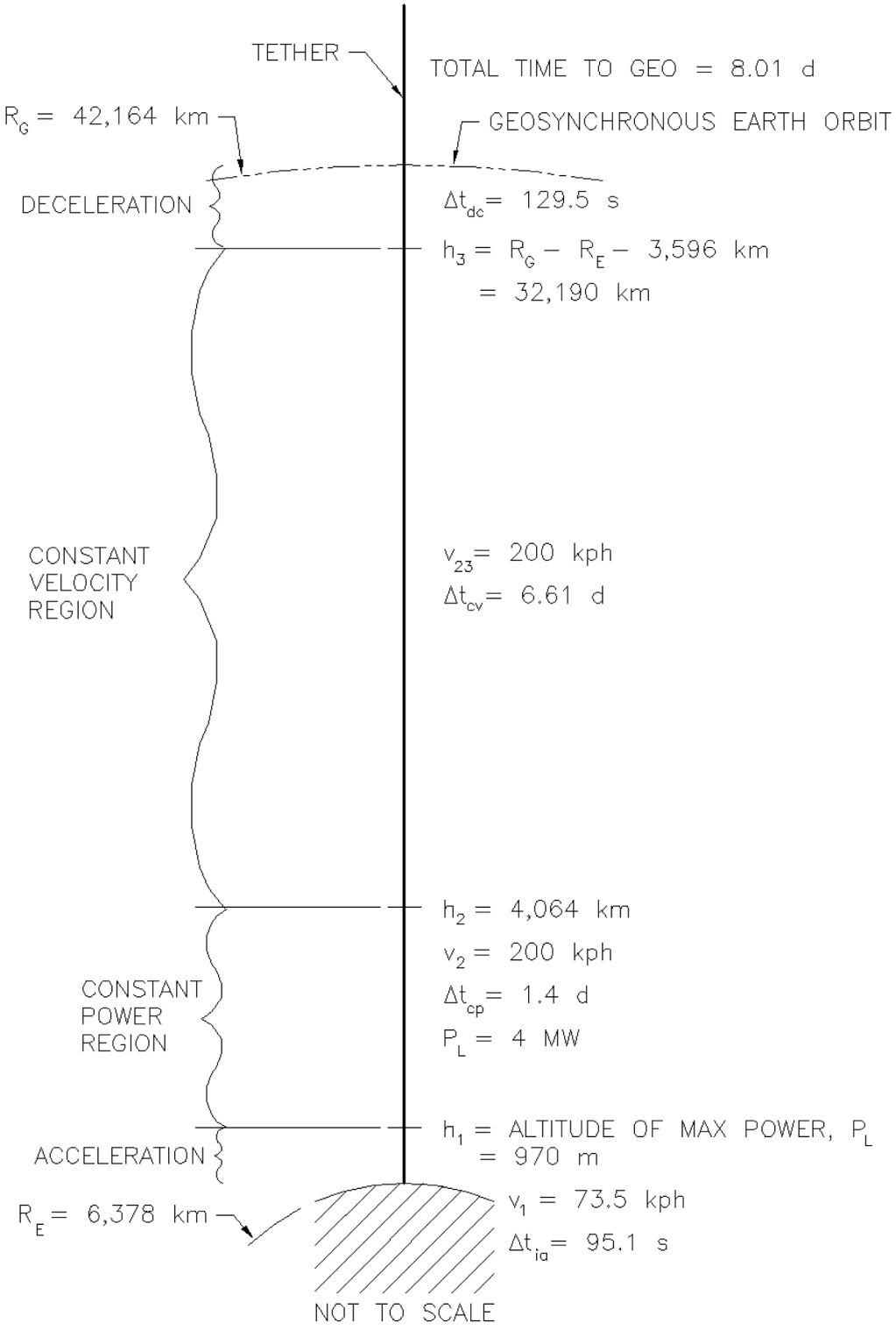

Fig. 2. Summary plot of altitude and time values for 8 day climb from Earth's surface to GEO.

where

$$a = 2\sqrt{\frac{F_c R_W}{\pi E^*}} \quad with \quad \frac{1}{E^*} = \frac{1-\nu_1^2}{E_1} + \frac{1-\nu_2^2}{E_2}. \tag{12}$$

F_c is the compressive force clamping the wheels together, R_W is the radius of the wheel and W_W is the width of the wheel. E_1 and E_2 are the Young's moduli of the tether and wheel materials, respectively, and ν_1 and ν_2 are the corresponding Poisson's ratios. The maximum pressure is

$$P_{max} = \sqrt{\frac{E^* F_c}{\pi R_W W_W}}. \tag{13}$$

Contact theory assumes that both the tether and wheels can be treated as solids. The wheels use cutouts to reduce mass, leading to a possible departure from behavior as a solid cylinder. This is likely a small effect and at any rate would increase the contact area, thereby

decreasing the maximum pressure. The tether will be very thin, about 10 μm at its thinnest. It is questionable, then, if it can be treated as a solid plane. An alternate calculation assumes that the tether can be neglected in determining the contact area and pressure. In that case, cylinder-on-cylinder contact must be calculated. Assuming that the two wheels are identical in radius and material, Eqs. (11)–(13) can be used, but with $E^* = E_2/(1-\nu_2^2)$.

Assuming titanium alloy (Ti–6Al–4V) wheels and a GSL tether, the two methods give similar results. For a 20 t climber, the clamping force is $F_c = 355{,}858\ N$ and the wheel dimensions are $R_W = 0.2794$ m and $W_W = 0.3$ m. For the tether material, $E_1 = 1$ TPa and $\nu_1 = 0.456$. For a titanium alloy wheel, $E_2 = 113.8$ GPa and $\nu_2 = 0.342$. The cylinder-on-plane contact area and pressure are then

$$A_c = 8.95\ \text{cm}^2\ ,\quad P_{max} = 397\ \text{MPa}. \tag{14}$$

For the cylinder-on-cylinder case, $E^* = 128.9$ GPa to get

$$A_c = 8.53\ \text{cm}^2\ ,\quad P_{max} = 417.4\ \text{MPa}. \tag{15}$$

These values are close to those for the cylinder-on-plane case. Since the maximum pressure is of interest, the cylinder-on-cylinder values will be used going forward.

Maximum Combined Stress

The only mechanical stress at the interface is pressure. An effectively rigid climber chassis and the choice of a pinched-wheel drive make torsion and bending negligible. Neither tension nor shear are intrinsic to the interface; each has different values on the tether side and on the wheel side. The applied stresses, tension, compression and shear, in the wheel are

$$\sigma_t = 0\ ,\ \sigma_c = P_{max}\ ,\ \tau = \frac{F_t}{A_c}\ , \tag{16}$$

where F_t is the tractive force from the wheel, and in the tether are

$$\sigma_t = \frac{\Delta T}{A_t}\ ,\ \sigma_c = P_{max}\ ,\ \tau = \frac{\Delta T}{A_c}\ , \tag{17}$$

where A_t is the cross sectional area of the tether and ΔT is the difference in tether tension above and below the climber.

The Mohr combined stresses will be functions only of σ_c, σ_t and τ:

$$\sigma_1 = \frac{\sigma_t+\sigma_c}{2} + \sqrt{\left(\frac{\sigma_t-\sigma_c}{2}\right)^2+\tau^2}\ , \tag{18}$$

$$\sigma_2 = \frac{\sigma_t+\sigma_c}{2} - \sqrt{\left(\frac{\sigma_t-\sigma_c}{2}\right)^2+\tau^2}\ , \tag{19}$$

$$\tau_{max} = \sqrt{\left(\frac{\sigma_t-\sigma_c}{2}\right)^2+\tau^2}\ , \tag{20}$$

where σ_1 and σ_2 are the principal maximum and minimum normal stresses and τ_{max} is the combined maximum shear stress. These values are limited by the maximum operating stresses of the tether and wheel materials.

2.2.3. Climber

Conditions for the climber include lift, wheel stress, available torque, the range of possible wheel radii and the rates at which heat is built up and dissipated. Lift, wheel stress and available torque depend directly on tractive force, while the wheel radius and heat have more complex dependencies.

Lift

The pinched-wheel reference configuration provides traction by symmetrical compression of the tether between two wheels. The tractive force F_t per wheel increases the tether tension above and decreases it below the wheel pair, causing a differential

$$\Delta T = 2F_t. \tag{21}$$

Table 1
Combined stresses in Ti–6Al–4V alloy.

Stress	Value (MPa)	Yield strength (MPa)[a]
σ_1	421.5	$\sigma_{ty} = 880$
σ_2	4.1	$\sigma_{cy} = 970$
τ	212.3	$\tau_y = 550$

[a]Values from Ref. [17].

Lift occurs when

$$N_{wp}\Delta T = 2NF_t > m_c[g(r)-c(r)]\ . \tag{22}$$

$g(r)$ and $c(r)$ are the gravitational and centrifugal accelerations at the equator as a function of altitude and N_{wp} is the number of wheel pairs of the climber.

At $r = R_E$, $g(r)-c(r) = 9.78$ m/s^2, so that a 20,000 kg climber has a force of (9.78 m/s^2)(2 ×10^4 kg) = 195.6 kN. For five wheel-pairs, the tractive force per wheel required to accelerate the climber is then $F_t >$ 19.56 kN, or a tension difference of 39.12 kN.

Wheel Stress Near the Interface

Eq. (16) gives the applied stresses in the wheel near its interface with the tether. Except for σ_t, these vary with altitude. From Eq. (11), P_{max}, and hence σ_c, is proportional to the square root of the axle clamping force F_c. Using Eqs. (9) and (12), the shear can be re-expressed as

$$\tau = \frac{F_t}{A_c} = \mu F_c/\sqrt{\frac{\pi R_W W_W F_c}{E^*}} = \mu\sqrt{\frac{F_c E^*}{\pi R_W W_W}} = \mu P_{max}\ , \tag{23}$$

so that the shear, too, is proportional to $\sqrt{F_c}$. F_c is largest at the Earth's surface, but can be reduced with increasing altitude as $g(r)-c(r)$ decreases. Maximum stresses, then, are to be calculated at the Earth's surface.

The applied stresses $\sigma_t = 0$, $\sigma_c = P_{max}$ and $\tau = \mu P_{max}$ are used in Eqs. (18), (19) and (20) to get the combined stresses, which must be less than the yield and shear strengths for the wheel material:

$$\sigma_1 = \frac{P_{max}}{2}[\sqrt{1+4\mu^2}+1] < \sigma_{ty}\ , \tag{24}$$

$$\sigma_2 = \frac{P_{max}}{2}[\sqrt{1+4\mu^2}-1] < \sigma_{cy}\ , \tag{25}$$

$$\tau_{max} = \frac{P_{max}}{2}\sqrt{1+4\mu^2} < \tau_y. \tag{26}$$

Table 1 shows the above stresses using $\mu = 0.1$ and $P_{max} = 417.4$ MPa, compared to the known material strengths from [17]. All the maximum stresses induced by the interface pressure and friction are well below the wheel material yield strengths.

Torque and Angular Momentum

In order to hold and accelerate a wheeled climber, each of the wheel drives must supply the tractive force F_t acting at a lever arm which is the wheel radius R_W:

$$M_m = F_t R_W. \tag{27}$$

Maximum torque will be required when the climber starts its ascent. The acceleration must be $g - c + a$, where $g - c$ is the net of the gravitational and centrifugal accelerations at the equator and a is the acceleration required to move upward. a is given by the wheel radius times the initial angular acceleration given in Section 2.2.1:

$$a = 0.768\ \text{s}^{-2} \times 0.2794\ \text{m} = 0.215\ \text{m/s}^2\ .$$

The total acceleration required is then about 10 m/s^2 (9.78 + 0.215) and the climber mass per motor is 2000 kg. The motor must supply a torque of $F_t \times R_W$ = 10 m/s^2 × 2000 kg × 0.2794 m = 5585 N-m or about 5600 N-m.

Table 2
Maximum fatigue stress (GPa) of Ti–6Al–4V alloy.

Cycles	1.2×10^5	1.0×10^7	4.8×10^8	8.2×10^9
50% C.L.	0.571	0.515	0.470	0.439
97.5% C.L.	0.487	0.429	0.384	0.353

At the point of lift-off, the angular velocity of a wheel is $\omega = 0$. Assuming the acceleration is constant at its initial, torque-limited value, ω increases linearly with time until maximum mechanical power (4 MW) is reached. At that point its value will be $\alpha_a \Delta t_{ia} = (0.768\ s^{-2})(95.1\ s) = 73\ s^{-1}$ or 697 RPM. The required torque falls off with increasing altitude so that, in the power-limited regime, ω increases to about 1900 RPM.

Wheel Radius

The climber wheel radius is a key design parameter, with a range of values limited by drive motor performance, material fatigue and axle spacing. The upper limit on the radius is imposed by the maximum torque that can be supplied by the motors,

$$R_W < \frac{M_{max}}{F_t}\ , \tag{28}$$

where F_t is the tractive force shown in Fig. 1 and M_{max} is the rated torque of the motor. The tare weight of the climber must be as small as possible, so the mass of the wheel could also limit the radius. However, with strong, lightweight materials and weight-efficient design, the torque provides a tighter upper limit. Purpose-built electric motors with masses around 200 kg can deliver 5700 N-m of torque [15]. With a tractive force $F_t = 19{,}620$ N per climber wheel, R_W could be as large as 0.29 m.

A lower limit on the wheel radius can be set by fatigue considerations. A climber wheel will make millions of revolutions on a trip to GEO. Each time a portion of the wheel surface comes into contact with the tether, the wheel is locally compressed and expands again after it rotates out of contact. The repeated flexing of the wheel material causes fatigue, which can be expressed as a stress. The maximum fatigue stress that a material can sustain decreases exponentially as a function of the number of cycles until it reaches a constant, infinite cycle value.

High-cycle fatigue stress is measured for many materials. Table 2 shows the maximum stress for titanium alloy Ti–6Al–4V at several cycle values. These values reflect the 50% confidence level, which means failure will occur 50% of the time when the given cycle number is reached. The 50% confidence level values were taken from [18]. For greater reliability, these values were converted here to the 97.5% confidence level.

To get an idea of how many cycles a wheel might survive, the 97.5% values should be compared to the average pressure at the wheel–tether contact patch. The contact pressure, supplied by the axle clamps, will be greatest at the surface of the Earth and decrease as the climber ascends into lower effective gravity. The pressure averaged over the trip to GEO is

$$P_{av} = f_{tav} P(R_E)\ , \tag{29}$$

where $P(R_E)$ is the contact pressure at Earth's surface and

$$f_{tav} = \frac{1}{R_G - R_E} \int_{R_E}^{R_G} dr \left(\frac{\mu_E}{r^2} - \Omega^2 r\right) \Big/ \left(\frac{\mu_E}{R_E^2} - \Omega^2 R_E\right) = 0.139. \tag{30}$$

Contact theory gives the pressure as a function of wheel radius. Taking the pressure in Eq. (11) to be the maximum fatigue stress S_f, an inequality for the wheel radius R can be found :

$$R_W > \frac{E^* F_c}{\pi w S_f^2}\ . \tag{31}$$

Applying the clamp force fraction f_{tav} and noting that $E^* = E/(1-\nu^2)$,

$$R_W > \frac{f_{tav} F_c}{\pi w S_f^2 (1-\nu^2)/E}\ . \tag{32}$$

From Table 2 it can be seen that the fatigue stress curve flattens out at very high cycles. The 97.5% CL values do not change much above 10^9 cycles, where they are between 0.35 and 0.37 GPa. Taking $S_f = 0.36$ GPa, $F_c = 355{,}858$ N, $w = 0.3$ m and $E/(1-\nu^2) = 129.1$ GPa, Eq. (32) gives

$$R_W > \frac{0.139(355{,}858\ \text{N})}{\pi(0.3\ \text{m})(0.36\ \text{GPa})^2/129.1\ \text{GPa}} = 0.052\ \text{m}\ .$$

With this minimum radius, a wheel would make 110 million revolutions on a trip to GEO and survive perhaps 100 such trips.

The wheel radius is thus bounded,

$$\frac{M_{max}}{F_t} > R_W > \frac{f_{tav} F_c}{\pi w S_f^2 (1-\nu^2)/E}. \tag{33}$$

Other considerations may constrain R_W further as the climber design evolves.

Climber Heating

Drive motor inefficiency, solar radiation, resistive losses in electrical buses and electronics, wheel–tether friction and elastic deformation of the climber wheels all contribute to the heat that builds up during climber operation. The heat must be dissipated at a rate sufficient to maintain the ambient climber temperature at reasonable operating levels for equipment and payloads. The only means to do this is by radiation since, for most of its journey, the climber is in vacuum.

Motor inefficiency and solar radiation are by far the largest sources of heat and the only ones that need be taken into account for a first estimate of the mass of a radiative cooling system. These, however, do not directly affect the climber–tether interface and will not be dealt with here.

Friction between the drive wheels and tether can be divided into two parts, sticking and slipping. In the sticking, or adhesion, region of the contact patch, there is static friction but no kinetic friction and therefore no energy loss. Kinetic friction occurs in the slip zone where the forward velocity of the axle v is larger than the product of the axle rotational velocity ω and the effective wheel radius R_{eff}. The fraction of the contact patch which undergoes kinetic friction can be estimated roughly by the slippage:

$$S = 1 - \frac{\omega R_{eff}}{v}. \tag{34}$$

The radius R_{eff} takes into account the deformation of the wheel as it is pressed into the tether, or the opposing wheel. Contact theory gives the value d of the deformation, so that

$$R_{eff} \approx 1 - \frac{d}{3R}\ , \tag{35}$$

where R is the undeformed wheel radius. Substituting Eq. (35) into Eq. (34) gives

$$S = 1 - \frac{\omega}{v}\left[R(1 - \frac{d}{3R})\right] = \frac{\omega d}{3v}. \tag{36}$$

The "slip velocity", $\frac{\omega d}{3}$ can be used to get the power of kinetic friction at its highest near the Earth's surface:

$$P_f = m_c g \mu \frac{\omega d}{3}\ , \tag{37}$$

with g the standard gravity, μ the coefficient of friction and m_c the climber mass. For titanium alloy wheels on a graphene tether, the wheel deformation d is about 11 μm. For $\mu = 0.1$, $\omega = 3000$ rpm and $m_c g = 196$ kN for a 20,000 kg climber, the power going into frictional heat is 22.6 W, a negligible amount.

Repeated deformation of the climber wheels as their surfaces rotate into and out of contact with the tether will be elastic rather than plastic. The resultant release of heat is therefore expected to be small and will be neglected in the current estimate.

Table 3
Maximum combined stresses in GSL tether.

Stress	Value (GPa)	Yield strength (GPa)	Citation
σ_1	18.58	σ_{ty} = 130	[20]
σ_2	0.417	σ_{cy} = 14	[21]
τ	9.08	τ_y = 0.14	[22]

2.2.4. Tether

Material

The primary tether candidate at this time is graphene super -laminate (GSL). Layered boron-nitride or carbon nanotubes are alternative candidates having different advantages and disadvantages. Tests of single-layer graphene demonstrate sufficiently high tensile strength (130 GPa) and low density (2260 kg/m^3) to support a space elevator tether and a number of climbers. Because this material is still under development, many of its properties are unknown. For example, it is very likely that multi-layer graphene, due to its layered structure, will not be isotropic. That is, the propagation of applied stresses through the material will depend on their direction. In the following discussion, however, isotropy is assumed simply because there are not enough data to define the anisotropic parameters. Details of the tether materials are discussed in Section 3. Known or estimated properties, with citations, can be found in the Appendix.

Tether Stress Near the Interface

Eq. (17) gives the applied stresses in the tether near the interface with the wheel. Using Eq. (21), these become

$$\sigma_t = \frac{2F_t}{A_t}, \quad \sigma_c = P_{max}, \quad \tau = \frac{2F_t}{A_c}. \tag{38}$$

σ_t decreases with altitude because F_t decreases and the cross section A_t increases with altitude up to GEO. Because maximum stress is of interest, this value can be taken at $r = R_E$,

$$\sigma_t = \frac{2F_t}{A_t} = \frac{2[g(R_E) - c(R_E)][m_c/(2N_{wp})]}{m_c[g(R_E) - c(R_E)]/\sigma_0} = \frac{\sigma_0}{N_{wp}}, \tag{39}$$

where σ_0 is the equilibrium stress, constant throughout the tether, m_c is the climber mass and N_{wp} is the number of wheel pairs. As in Eq. (23), τ remains constant,

$$\tau = 2\mu P_{max}. \tag{40}$$

Using Eqs. (18)–(20), the Mohr combined stresses are then

$$\sigma_1 = \frac{\sigma_0/N_{wp} + P_{max}}{2} + \sqrt{\left(\frac{\sigma_0/N_{wp} - P_{max}}{2}\right)^2 + 4\mu^2 P_{max}^2} < \sigma_{ty}, \tag{41}$$

$$\sigma_2 = \frac{\sigma_0/N_{wp} + P_{max}}{2} - \sqrt{\left(\frac{\sigma_0/N_{wp} - P_{max}}{2}\right)^2 + 4\mu^2 P_{max}^2} < \sigma_{cy}, \tag{42}$$

$$\tau = \sqrt{\left(\frac{\sigma_0/N_{wp} - P_{max}}{2}\right)^2 + 4\mu^2 P_{max}^2} < \tau_y. \tag{43}$$

The stress σ_0 should be set within the proportional region of the stress/strain curve of the tether material, which for graphene could be as low as 65 GPa, or half its ultimate tensile strength. To estimate the maximum stresses likely to occur during operation, σ_0 in the above expressions should be replaced by the ultimate tensile strength divided by a safety factor. Using the NASA standard for spacecraft [19], a factor of 1.4 is applied to get 130/1.4 = 92.9 GPa. Using this value, with μ = 0.1, P_{max} = 0.4174 GPa and N_{wp} = 5 in Eqs. (41)–(43) gives the maximum values of the combined principal stresses at any wheel–tether interface. These are listed in Table 3 where they are compared to the ultimate strengths of graphene.

The large tensile strength dominates, so that the total tensile and total compressive stresses are very little changed from the applied stress values, and are well below the material yield strengths. The combined shear stress, however, is about 65 times that of the measured shear strength of SCG. The shear strength of multi-layer graphene must be increased at least 100 times for it to be used as the tether material. Means of accomplishing this are discussed in Section 3.

2.3. Summary

Local climbability can be defined by the following conditions.

- *Friction:* the coefficient of friction between the wheel and tether surfaces must exceed a practical minimum.

  $\mu > \mu_{min}$.

- *Interface Temperature:* the temperature at the interface must be less than the maximum service temperature of either material.

  $T_{interface} < min(T_{maxW}, T_{maxT})$.

  where T_{maxW} and T_{maxT} are the maximum temperatures for the wheel and tether, respectively.
- *Combined Stress:* combined stresses depend on interface pressure, contact patch area and differential tether tension, and may not exceed maximum operating values.

  $$\sigma_{ttot} = \frac{\sigma_t + \sigma_c}{2} + \sqrt{\left(\frac{\sigma_t - \sigma_c}{2}\right)^2 + \tau^2} < \sigma_{tmax},$$

  $$\sigma_{ctot} = \frac{\sigma_t + \sigma_c}{2} - \sqrt{\left(\frac{\sigma_t - \sigma_c}{2}\right)^2 + \tau^2} < \sigma_{cmax},$$

  $$\tau_{tot} = \sqrt{\left(\frac{\sigma_t - \sigma_c}{2}\right)^2 + \tau^2} < \tau_{max},$$

  where the applied tensional stress is

  $$\sigma_t = \begin{cases} \Delta T/A_t & for\ tether \\ 0 & for\ wheels \end{cases},$$

  the applied compressive stress is

  $\sigma_c = P_{max}$

  and the applied shear is

  $$\tau = \begin{cases} \Delta T/A_c & for\ tether \\ F_t/A_c & for\ wheels \end{cases}.$$

- *Lift:* the difference in tether tension induced by tractive force must exceed the difference of gravity and centrifugal force.

  $$N_{wp}\Delta T = 2N_{wp}F_t > m_c[g(r) - c(r)], \tag{44}$$

  where N_{wp} is the number of wheel pairs, $2N_{wp}F_t$ is the total tractive force due to all wheels and $N_{wp}\Delta T$ is the total difference in tension above and below the climber. m_c is the climber mass and $g(r)$ and $c(r)$ are the gravitational and centrifugal accelerations.
- *Motor Torque:* total motor torque must exceed the product of initial tractive force and climber wheel radius.

  $$M_{total} > F_t R_W, \tag{45}$$

  where R_W is the wheel radius and $M_{total} = 2N_{wp} * M_m$. N_{wp} is the number of sets of opposing wheels comprising the climber and M_m is the maximum operating torque of the motor driving each wheel.
- *Wheel Radius:* the wheel radius must be large enough to avoid high–cycle stress failure and smaller than the motor torque per tractive force.

  $$\frac{M_{total}}{F_t} > R_W > \frac{F_{cav}}{\pi W_W p_F^2 (1 - \nu^2)/E}, \tag{46}$$

  where F_{cav} is the applied compressive force averaged over the trip to GEO and W_W is the width of the wheel. The remaining parameters are properties of the wheel material, with p_F the fatigue pressure as a function of the number of wheel rotations, E the Young's modulus and ν the Poisson's ratio.

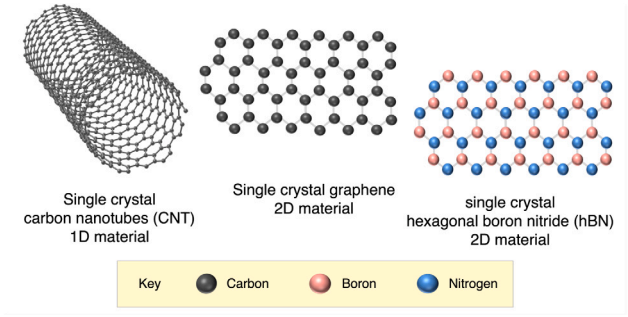

Fig. 3. Molecular structure of candidate tether materials.

3. Tether characteristics

3.1. Purpose and status

The space elevator tether has two functions: to support itself and to raise payload. The sum of climber masses will be small compared to the total tether mass, but the stresses their drives exert on the tether will be significant. As yet, no material of sufficient strength exists in large enough quantities to serve these functions, but the prognosis for mass production of such materials in the near future is good.

Candidate materials for the tether are carbon nanotubes (CNT), graphene super-laminate (GSL) and hexagonal boron nitride (hBN). Laboratory samples of each of these have been produced with sufficient specific strength [23], but kilometer-scale lengths will be required so that they can be spliced together to make a 100,000 km long tether.

Until recently, CNTs appeared to be the prime candidate for the tether material, however, progress in making longer lengths seems to have stalled. Proposed manufacturing processes for the 2D materials, GSL and hBN, seem to have no limits on the lengths or speeds at which they can be produced. This, and the fact that 2D materials seem geometrically best suited to the construction of an essentially 2D tether, make GSL or hBN the preferred options.

3.2. Materials

There are three candidate materials with the required strength. These materials are described as single crystal. Crystal in this context refers to an uninterrupted repeating pattern at the molecular scale and is a single molecule of material that will produce the maximum strength possible. Where defects and vacancies are present the material is described as polycrystalline, and the material has a lesser strength. The molecular structures of single crystal carbon nanotubes, single crystal graphene and single crystal hexagonal boron nitride (hBN) are shown in Fig. 3.

These materials can be classified as one dimensional (1D) or two dimensional (2D). Dimensions in this context refers to the number of spatial dimensions in which a molecule can grow while still retaining the same characteristics. For example, carbon nanotubes can grow from either end of the tube, provided it is not capped, and remain the same material. If extra carbon atoms were to be added to the sides of the tube this would change the nature of the material. Similarly, graphene and hBN can only grow in the x and y dimensions with atoms attached by covalent bonds.

3.2.1. Graphene super-laminate

Multi-layered single crystal graphene consists of layers of single crystal graphene stacked in such a way as to maximize the Van der Waals forces between them. To simplify the language, the term graphene super-laminate (GSL) is used here to mean a Van der Waals homostructure of multi-layered, single-crystal, large-area graphene.

Each layer is a single molecule of sp2 hybridized carbon 0.335 nm thick [24]. To create a tether of sufficient strength, tens of thousands of such molecules will need to be laid on top of one another. This thickness assumes a 20 t climber departing Earth each day on a tether up to one meter in width. To increase the mass raised, either the tether thickness or width must be increased. The most stable, and strongest, of the possible layering orientations is called AB stacking. A stick-and-ball model of this configuration is shown in Fig. 6. Graphene layers in AB stacking will not slide by one another as easily as they do in alternative configurations such as AA stacked or randomly stacked (turbostratic) graphene [25].

In addition to its high tensile strength (130 GPa) [20] and low density (2298 kg/m3) [9], GSL offers many other useful properties including high electrical and heat conductivity, high current density, and good resistance to chemical attack by free radicals. Of direct relevance to the climbability condition, graphene can sustain very high compressive forces, up to 14 GPa [21]. This is much higher than the climber wheels will exert.

Graphene, however, is rather slippery, with a recently measured coefficient of friction of 0.1 [26] (Table A.1). This value is on the low side for a pinched-wheel climber design and modifications to the surface of a GSL tether may eventually be required [23]. The resistance of GSL to shear forces is also on the low side with a shear modulus between 0.19 and 0.49 GPa [27].

3.2.2. Hexagonal boron nitride

Hexagonal boron nitride (hBN) is another 2D material in which boron and nitrogen atoms are arranged in a hexagonal pattern. Fig. 3 shows the structure. It has a lower strength, 100.5 GPa [28], than GSL, but this is somewhat compensated by a lower density (2.0 to 2.2 g/cm^3 [29]) and higher interlayer shear strength (3.07 to 4.31 GPa [27]). hBN has a relatively high thermal conductivity, 751 W/m/K [30], but unlike GSL it is a good electrical insulator. It is in many ways complementary to GSL; where more friction or insulation is needed, hBN could be used, having a coefficient of friction between 0.23 and 0.27 [31] (Table A.1), and where more strength or electrical conductivity is needed GSL could be used.

3.2.3. Carbon nanotubes

Although not examined in this study, carbon nanotubes (CNTs) were the first of the strong materials to be proposed for constructing the space elevator tether. It is useful to compare their properties to those of GSL and hBN. CNTs come in many varieties depending on the pattern of the carbon atoms and the number of atomic layers (walls). For simplicity only single-walled carbon nanotubes (SWCNT) are discussed here. SWCNTs have the same strength as GSL (Table A.1), but a lower density than either GSL or hBN, which is a distinct advantage. The coefficient of friction is similar to that of hBN, so it is easier to grip. SWCNTs have a very good electrical conductivity, but not as high as GSL. Thermal conductivity appears to be better than that for GSL.

In the laboratory, SWCNTs and single crystal graphene have been produced with similar lengths (0.5 m), so it would appear that they are both good candidates for the tether material. GSL was chosen for this study because of the greater likelihood that it could be produced in longer lengths, at higher rates and at an earlier date.

3.2.4. Tether materials comparison

For quick comparison, several properties of the three tether materials are listed in Table 4. They are: tensile strength, σ_{TS} in GPa; shear strength, τ_{SS} in GPa; coefficient of friction, μ; and bulk density, ρ in kg/m^3. A full list of known and estimated material properties is included in the Appendix.

3.3. Materials manufacturing

To achieve a focus on the material of choice, the state of the art of manufacture of these materials was reviewed.

Table 4
Comparison of selected mechanical properties of tether materials.

Material	σ_{TS}	τ_{SS}	μ	ρ
GSL	70–130	0.14	0.03–0.1	2290
hBN	100	3.1–4.3	0.23	2200
SWCNT	77–200		0.22–0.24	1600

Fig. 4. General Graphene Inc. roll-to-roll graphene production line. Image credit: General Graphene.

3.3.1. Carbon nanotubes

Carbon nanotubes are manufactured industrially. OCSiAl, a Luxembourg-based manufacturer has a carbon nanotube production capacity with its Tuball subsidiary company that is stated to be 90 t of CNTs per year. The company says this accounts for over 97% of the global graphene nanotube market. However, the carbon nanotubes it produces are just 5 μm in length and seem to be used as powdered additives to enhance the performance of other materials [32].

Longer CNTs have only been made in the laboratory. The longest single-molecule carbon nanotube made so far is 0.5 m in 2013 [5]. Since then no further improvements in length have been reported. The state of the art of carbon nanotube manufacture seems to be to make nanotube forests with a length of 0.14 m and probably polycrystalline [33].

3.3.2. Hexagonal boron nitride

Large-area sheet hBN is produced industrially. The most prominent manufacturer is Grolltex Technologies in California, USA. The company has developed a batch process that manufactures hBN by a CVD method on metal foil and can transfer the material to other substrates. However, this is restricted to 200 mm diameter wafers for the semiconductor industry [34].

3.3.3. Large-area sheet graphene

The industrial state of the art making large area graphene is capable of manufacturing polycrystalline material. The industrial manufacture of single crystal has yet to be attained. However, progress has been astonishing, and several industrial companies have developed scaleable processes making polycrystalline material.

General Graphene Inc., based in the USA, has announced that its Gen 3.0 roll-to-roll graphene production line has been commissioned and can make 100,000 m^2 of graphene on copper foil per year [35]. Fig. 4 shows the production line.

General Graphene has also demonstrated the ability to separate the graphene from the copper foil and create multilayered graphene samples on a transparent plastic film substrate. The company provided samples to ISEC as shown in Fig. 5.

In South Korea, two companies have created industrial-scale graphene manufacturing plants. LG Corporation has developed a roll-to-roll production method that can make graphene on copper foil at speeds of up to one meter per minute and lengths of up to one kilometer [35]. Charmgraphene has gone further and can produce graphene on copper foil at speeds of two meters per minute and lengths of one kilometer [35]. The company has also automated the separation of graphene from the copper foil and transfer to other substrates.

Charmgraphene has also demonstrated the ability to separate graphene from the copper foil surface. They can create free-standing multi-layered graphene [36]. Free-standing means there is no substrate support; the atomic layers of graphene support themselves. The multi-layered graphene is 110 mm wide by 144 mm in length.

While industrial manufacturers are making polycrystalline graphene, work continues on making single crystal graphene in the laboratory. The longest sheet of single crystal graphene was made at a scale of 500 mm by 50 mm at Peking University, Beijing, China in 2017 [3]. The largest area of single crystal graphene to date has been reported by researchers from Oak Ridge National Laboratory, who demonstrated the manufacture of single crystals of 300 mm by 300 mm area [37].

3.3.4. Manufacturing summary

To make the material for the space elevator tether requires manufacturing on very large scales and speeds. Carbon nanotubes can be made at sub-meter lengths, very slowly. Hexagonal boron nitride can be made industrially but only at a scale of 200 mm in diameter for electrics applications.

Graphene on the other hand can already be made at lengths of one kilometer and a speed of two meters per minute. None of these materials can be made at tether quality yet, however the trajectory clearly favors graphene as the industrial material of choice, and this is why graphene was the focus of attention for this study.

3.4. Design considerations

Assuming that the basic tether material will be made available, the next step will be to determine how it should be structured. The tether will not consist of a monolithic and isotropic block of material, but rather of laminations of thin layers or weavings of thin tubes spliced together. The final design will depend on the basic material properties, the stresses and environmental conditions to which the materials will be subjected and the details of the tether assembly process.

3.4.1. Requirements

Stresses

The requirements for the tether material in the vicinity of the climber can be taken from the combined stresses listed in Table 3. Implicit in the climbability requirements was that the tether could sustain a tension of $\sigma_{TS} = 130/1.4 = 92.9$ GPa, where 1.4 is the safety factor. Thus it was assumed that the applied tensile stress was never more than 92.9 GPa. The resulting combined tensile stress per wheel pair was 18.58 GPa, well below the yield strength.

Resistance to shear forces is a critical requirement; the downward force due to climber mass on the surface of the tether must not exceed the force holding the layers together. The maximum combined shear force at the interface was found to be 9.08 GPa, 65 times larger than the measured shear strength of 0.14 GPa.

The compression of the tether due to the wheels must not exceed the compressive strength of the tether. The combined compressive stress was found to be 0.417 GPa, well below the quoted yield strength of 14 GPa. Comparing this to the 0.88 GPa compressive strength of titanium wheels (Table 1), it is the wheels and not the tether that set the maximum allowed compression at around 0.9 GPa.

For the tether material in the immediate region of the climber, there are no requirements concerning bending or torsional stresses. Having chosen not to use a capstan drive, the tether will not be subject to

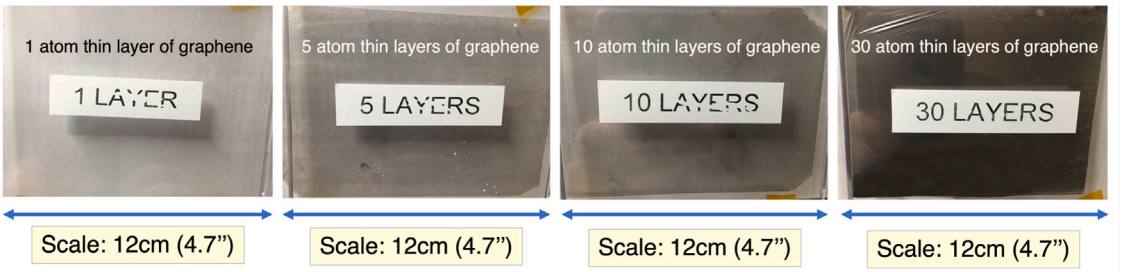

Fig. 5. Samples of multiple graphene layers made for ISEC. This is not tether quality graphene and is meant only to show the pace of manufacturing development. Image credit: Michael Fitzgerald (International Space Elevator Consortium).

bending moments. The climber frame which holds the wheel pairs in place will prevent any significant torsion.

Environmental Conditions

The tether will be immersed in a variety of environments including atmosphere, vacuum, electromagnetic fields, radiation fields and thermal gradients.

Corrosive chemicals in the Earth's atmosphere will degrade the tether. Salt water and water vapor at low altitudes and oxygen radicals at higher altitudes will react with the tether materials and decrease their strength. While a single layer of graphene has every one of its atoms exposed to its environment, the great bulk of the atoms in GSL will be insulated due to its many tightly packed layers. Only the surface layers and edges will be vulnerable to chemical reactions. The same is likely to be true for hBN. In both cases, edge reactivity could be suppressed by folding or rolling. A single CNT exposes all of its atoms as well. Reactivity could be reduced by braiding the CNTs, but this is unlikely to remove as many atoms from environmental contact as in the case of GSL.

The large electrical conductivities of GSL and CNTs mean that significant currents and forces may be induced in the tether by Earth's electromagnetic fields. These can result in displacements of thousands of kilometers at the apex when extreme solar storms arise, but usually such oscillations are small and certainly negligible in the immediate region of the climber. This issue could even be eliminated by building a tether partially or entirely with hBN, which is an insulator. There are, then, no particular electrical requirements of the materials in this respect.

Thermal gradients are certain to occur along the tether length and particularly in the region of the climber where friction with the wheels will induce heat at the contact areas. High thermal conductivity in the tether will mitigate this problem.

The radiation environment will be severe. Hard ultraviolet and particle irradiation is ubiquitous in space and the upper atmosphere and the tether materials must be resistant to it. The tensile strength of CNT yarns was reduced by about 50% after a long exposure to space radiation [38]. GSL may perform better in such circumstances since the carbon atoms in laminations would be packed more closely together than in CNT braids, thus retaining more strength when atomic bonds are destroyed.

Assembly Conditions

The basic material will be manufactured on Earth in the form of sheets of GSL or hBN, or fabrics of woven CNTs. The lamination of GSL and hBN layers into thicker sheets requires a good vacuum environment in order to avoid intercalation. This argues for the lamination to be done in space, requiring an assembly satellite in GEO. Rolls of the basic material must be transported to space by rocket and therefore must fit into available cargo holds. The proposed tether width poses no problem in this regard and the thinness of each layer means that a very large number of sheets would fit into a single roll of manageable mass.

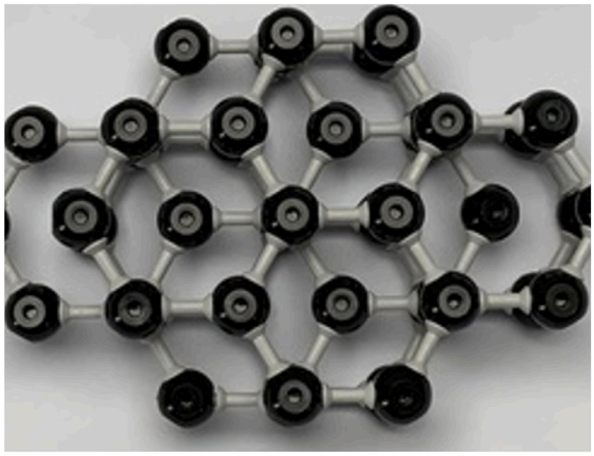

Fig. 6. View looking down on a model of AB stacked multi-layer graphene. Each alternate carbon atom in a six-atom ring is located directly above the center of a ring directly below it.

3.4.2. Lamination

The most straightforward option for building a tether out of 2D materials is lamination. Given their nanometer-scale thickness, thousands of layers will be required to construct a practical tether.

Natural Bonding

Layers of single crystal graphene will naturally adhere to one another by Van der Waals bonding to form GSL. The bonding arrangement with the smallest distance between layers is called AB stacking which is illustrated in Fig. 6. The Van der Waals forces are strongest in this arrangement and would provide the most resistance to shear stress.

Spot Welding

If the Van der Waals forces are not strong enough, large shear forces on the surface of the tether material will not be sufficiently distributed into the bulk and de-lamination will occur. According to Table 3 the shear strength of GSL is 0.14 GPa, about 65 times too weak to support the climber. Thus, another bonding option must be considered.

In GSL, the carbon atoms are connected by hybrid sp2 bonds. The remaining π orbitals are unbonded and oriented perpendicular to the plane of the graphene layer. When two such layers are pressed together, the sp2 bonds and π orbitals create sp3 bonds between the layers, as shown in Fig. 7. The sp3 hybrid bond is the one found in diamond and accounts for its strength. The pressure at which this type of bonding occurs is thought to be about 23 GPa [21]. Ultrafast lasers can achieve such pressures and have been used to synthesize the diamond phase (sp3 bonds) from the layered phase (sp2 bonds) [39]. It has also been shown recently that when several atoms take part in this bonding, the results are irreversible [40]. Perhaps this process could be applied on an industrial scale to produce a material resistant to the shear stresses expected in the space elevator tether.

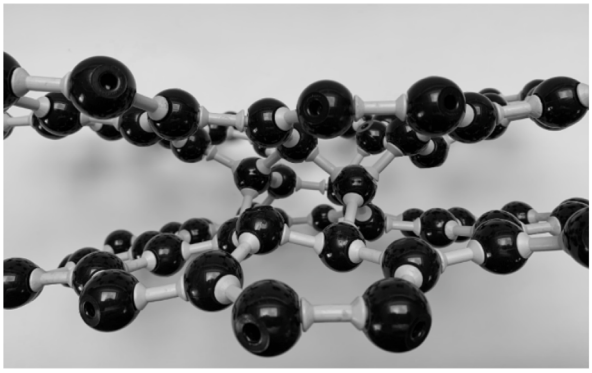

Fig. 7. Stick-and-ball model of "spot-welded" multilayer graphene. The sp3 hybrid bonds are shown in the center, between two layers of graphene.

Increasing Friction

Research for this study discovered that reliable figures for friction in 2D materials are not easily found and that the literature contains a wide range of values from 0.03 to 0.1 [26,41] (Table A.1). These values were obtained using atomic force microscopy in which a diamond tip is dragged over the sample surface. The view of the study group was that fresh work needs to be conducted using a metal-coated tip against the graphene surface. Larger scale tests are preferred when macroscopic samples can be obtained. This would replicate the conditions of a climber wheel against a graphene tether more reliably. A coefficient of friction value of 0.1 was chosen for this study as it was the most recently measured.

However the lamination is done, the surface of the tether is likely to be rather smooth, with a coefficient of friction of about 0.1. This is a manageable number in mechanical engineering, but on the edge of practicality for friction drives in space elevator climbers.

Two methods may be able to raise the effective coefficient of friction. One is to introduce hydrogen onto the surface of the GSL. Measurements show that this increases the coefficient of friction to about 0.13 [42]. Another method would be to use hBN as an outer layer bonded to a tether bulk consisting of GSL; GSL and hBN naturally bond to one another forming a Van der Waals heterostructure [43]. According to Table A.1, hBN has a coefficient of friction of about 0.25, which would provide much more holding force between the climber wheels and tether. Other methods involve making the surface rougher by the creation of diamond studs at regular intervals using high pressure, and wrinkling or creping the surface.

3.4.3. Braiding

Another option is to construct the tether using CNTs or rolled-up GSL or hBN layers. These tubular structures would be braided into threads and woven to create the tether fabric. This method has two advantages. Because the tubular molecular structure has no edges, it is highly resistant to attack by oxygen radicals and other chemicals in the atmosphere. Also, sheets produced by braiding and weaving would create a rougher surface with a much higher coefficient of friction for the climber wheels. The main disadvantage is that a braid is always weaker than its component threads.

3.5. Molecular modeling

The methods listed above for increasing shear strength and the coefficient of friction are conjecture based on some recent measurements. They have to date not been attempted in any manufacturing process. Absent this, it is useful to see if computer modeling can shed some light on the possibility of these processes. Molecular modeling can be used to see how macro-molecules interact with each other and with their environments.

The key requirement of such modeling is the prediction of macroscopic material properties and the formation and propagation of defects, based on the electromagnetic interactions of individual molecules. The list of properties to be modeled and predicted include the coefficient of friction between graphene sheets and other materials, and the multi-axial tensile, shear and compression strengths of single and multiple graphene layers. Also to be modeled are the formation of defects and their propagation, the adsorption of gasses, the effects of pressure and temperature and the effects of the various stacking configurations of graphene sheets.

Two calculations would be of immediate interest for the GSL manufacturing process: calculation of the adsorption of hydrogen onto graphene is one possible way to predict how the coefficient of friction of the modified material would vary with hydrogen concentration; the introduction of localized pressure at intervals along the length of a two-layer graphene structure would indicate whether or not sp2 bonds in the two sheets could be converted to sp3 bonds between sheets, thus allowing the "spot-welding" of layers.

It is also essential to understand how defects are formed and propagated under the various stresses that will be applied to the tether material. Knocking carbon atoms out of their hexagonal pattern and the introduction of irregularities that could show up during manufacturing need to be simulated as well as how these irregularities develop into strength-reducing tears in the material.

In principle, all of these calculations can be done, but the major challenge, and one reason that these calculations have not been done, is that large numbers of atoms must be included in the calculation space in order to make predictions of macroscopic parameters. This is likely to require advanced computational methods and super-computers. Several approaches to this problem and the computer codes required are discussed in Section 5.

3.6. Proposed tether design

There are several candidates for the material from which a space elevator tether may be constructed. Based on requirements from climbability and climber design, and speculation about the internal structure of the tether, a preliminary tether design is presented here.

An essentially two-dimensional structure will consist in its bulk of tens of thousands of layers of AB-stacked single crystal graphene with its shear strength augmented by periodic spot welding between the layers. Several layers of hexagonal boron nitride will be laminated on either face of the GSL ribbon in order to provide increased friction and radiation hardness. These layers will also be cross-linked to layers beneath them by spot welding. To prevent chemical reactions at the edges of the molecular layers, it may be possible to use much wider layers and fold them accordion-style before binding them together.

An alternative geometry of woven braids of CNTs or GSL/hBN tubes would provide greater friction for the climber wheels and resistance to chemical attack, but would likely lack the necessary tensile strength for supporting itself.

4. Projected tether improvements

The study identified a number of areas in which improved technology would enhance the ability of the space elevator to carry payload. These improvements can be made with technology that exists or is likely to exist in the next decade. Areas of research which underpin the anticipated technologies were also identified and will be discussed in Section 5.

Development in the world of graphene and other two-dimensional (2D) materials has been rapid. Prior to 2004 graphene was considered purely theoretical. Since then, graphene has moved from the laboratory to industrial scale manufacturing; it can now be made in lengths of up

to one kilometer and at speeds of two meters per minute. However, this material is polycrystalline and contains defects which limit its use for high-strength applications; it is not tether-quality material yet.

This progress of industrial manufacturing of graphene is not limited to one location or organization. At least three separate organizations in Asia and North America have publicly declared their development work. There are other organizations actively involved in making tether-quality material who have asked not to be named.

The successes in manufacturing graphene could prompt other researchers to revisit the manufacture of carbon nanotubes, hexagonal boron nitride (hBN) nanotubes and also hBN super laminate.

The rate of development seems set to continue, and it is reasonable to assume that high quality GSL material suitable for the tether will be made within the next decade.

4.1. Coefficient of friction

The current study has revealed that measuring friction is not as straightforward as it might first appear. The peer-reviewed literature contains a wide range of values for the coefficient of friction for the candidate tether materials.

This variation is partly due to limitations of the measurement techniques owing to the small samples of material generally used. The study also came to the view that a meaningful measure of friction is best performed using the same materials that will be used for the tether and the climber wheel surfaces.

As far as could be determined, no study investigating the friction between titanium and GSL has been performed. This should be possible in the foreseeable future as material samples become available. The authors encourage researchers to perform these tests and make their results public.

4.2. Shear strength

The mechanical stresses between the climber and tether also indicated that there will be significant shear forces on the tether. A tether made of layers of 2D material or braided nanotubes will need to withstand these forces. The layers in a 2D material are held together by Van der Waals forces. Experimental evidence for the behavior of these layers under shear is very limited. This study has also found that computer modeling of the Van der Waals force needs much more work and researchers are encouraged to direct effort in both these areas in the coming years.

5. Proposed research

5.1. Molecular modeling

The macroscopic properties of graphene and GSL of most interest in the construction of a space elevator tether are: the coefficient of friction between graphene sheets and between graphene and other materials, the multi-axial tensile, shear and compression strengths of single and multiple graphene layers, the formation of defects and their propagation, the adsorption of gasses, the effects of pressure and temperature and the effects of the various stacking configurations of graphene sheets.

In the absence of measurement, molecular modeling must be used to predict these properties. Modeling includes the specification of the molecular structure and the calculation of its dynamics, that is, the state of the molecule as a function of time. From this, the forces on atoms, the effects of pressure and temperature, possible failure modes and so on, can be predicted.

Molecular modeling is a broad and primarily computational area of research consisting of many theoretical approaches depending on the application. In the case of graphene, the behavior of large molecules under various conditions is desired. For such large molecules, the classical molecular dynamics approach is preferred over the quantum mechanical because it can handle a larger number of atoms (~100,000) and takes less CPU time. Graphene is not a simple molecule, though, so a quantum code may eventually be required.

Software Packages

Three classical software packages that may apply are SAMSON [44], LAMMPS [45] and GROMACS [46]. The quantum mechanical code VASP [47] might also be used. These packages allow molecules to be built and simulated using molecular mechanics and dynamics. Individual atoms can be moved around, removed or added to existing molecules. For example, one layer of graphene can be moved with respect to an adjacent one. Various temperatures and pressures can also be applied to the modeled sample. When such changes are made, the codes do automatic force minimization to get the lowest energy configuration.

Classical calculations model atoms as mass points and the bonds between them as springs. Non-bonded forces such as Coulomb and Van der Waals are also modeled. These are summed to create a potential from which forces are derived. Each of these codes provides or allows for different types of interaction models or force fields. Force fields are required in order to describe the interaction between atoms and to calculate the forces and energies in the system.

SAMSON, for example, can use the Brenner force field model [48] which simulates bond formation, breaking and reactions. This would be particularly useful in studying the formation of the sp3 bonds required to spot-weld together layers of graphene within GSL. It could also help to understand how defects and tears in large graphene sheets form and spread under stress. Ideally, this would provide an indication at the molecular level of when macroscopic failure was about to occur.

GraFF (Forcefield for Graphene and Graphite) [49] is an interaction model to be used with LAMMPS. It was developed to address problems with existing simple Lennard–Jones potentials in representing graphene–graphene interactions. A typical problem for many molecular modelers is poor Van der Waals interactions which often lead to incorrect potential energy surfaces. GraFF has purpose-built Van der Waals interactions based on the Lennard–Jones potentials. This is important for studies of friction between graphene sheets or other materials because friction arises from the Van der Waals interaction. GraFF can also calculate the sustainable shear stress in GSL. One caveat here is that the Lennard-Jones potential will work for carbon, but it is not known yet if it works for hBN.

In the quantum mechanical approach, calculations are based on either Hartree–Fock methods or density functional theory. The Hartree–Fock method is a means of approximating the wave function and the energy of a quantum many-body system. It is used to solve the Schrodinger equation for atoms and molecules.

Density functional theory [50] (DFT), is also an approximate method in which the electron density is the fundamental property, instead of the wave function. It allows the interaction potential of an N-electron system to be expressed as the sum of N single-electron potentials, thus greatly simplifying the calculations. Being an ab initio theory, material parameters are not required as input.

VASP is a simulation package for materials modeling which can calculate electronic structure and quantum molecular dynamics from first principles. It can calculate internal forces and stresses, response to ionic displacements (elastic constants) and response to electric fields such as dielectric properties.

A Possible Approach to Modeling Graphene and GSL

The modeling of graphene and GSL would probably best be approached by a hybrid quantum–classical calculation. A quantum calculation would be most accurate, using Schrodinger's equation and DFT. It is, though, CPU intensive and usually cannot accommodate large numbers of atoms. The modeling would probably start with a Hartree–Fock calculation, as this is a detailed quantum-mechanical approach. Only 30 to 50 atoms could be modeled, but it would tell us what

approximations could be made in going to larger structures. It could be used to develop a DFT for graphene, which could then be used in the classical calculation to minimize the potential energy in order to get the molecule's ground state and compare to other states. Doing the rest of the calculation with the classical GraFF code would allow orders of magnitude more atoms to be simulated with a smaller expenditure of CPU time. It is also possible that a machine learning approach could be used, which would blend the classical and quantum approaches.

The initial model development may still be very CPU intensive and require a supercomputer. However, once the model is developed, the dynamics calculations could be performed on personal computing devices.

5.2. Material properties

Only a few basic tether material properties, summarized in the Appendix, are known at this time. This state of affairs will soon change as new measurements and experiments appear, but for the time being, scalar parameters like tensile strength, shear strength, coefficient of friction, heat conduction and electrical conduction must suffice for all designs and calculations pertaining to the climber–tether interface. It was assumed in this report that the above parameters are isotropic, that is, their values do not depend on the directions of forces in the tether and at the interface. This will certainly not be the case for any of the candidate tether materials, but is assumed to be so due to the lack of anisotropic measurements.

The nature of the anisotropy in these materials can be guessed based on the molecular structure and the way in which the molecules are assembled to form the tether, but measured values are essential. The most-needed measurements and proposals for how these might be obtained are listed below.

5.2.1. Anisotropic parameters

Anisotropic material parameters depend on the direction of forces in the material. If the material is isotropic, one parameter is sufficient to describe, for example, tensile strength. The material can be treated as uniform in all directions. A non-uniform material will respond differently to forces in different directions and in general will require many more parameters to describe the response.

A fully anisotropic material requires 21 independent parameters to describe, say, its elastic response. However, most materials have symmetries which greatly reduce the number of parameters needed. Laminates, for example, exhibit transverse isotropy in which the material is isotropic in the plane of the layer, but not in the direction perpendicular to the layer. Such materials require only five parameters to describe the response. In orthotropic materials there are three mutually perpendicular directions in which the properties are different. Wood is a good example of this, having symmetry about the ring axis, along the grain and along the ring radius. Nine parameters are required for such materials.

Graphene super-laminate (GSL) may be likened to thin layers of honeycomb glued together in a stack. The honeycomb cell structure is known to be transverse isotropic [51], so the stack must be also, as long as the layers are aligned in certain ways. In Section 3.4.2, the concept of cross-bonding the molecular layers in GSL was discussed as a method of improving its shear strength. Assuming that the cross-bonds are made at regular intervals along the length of the layer, another anisotropy will be introduced perpendicular to both the thickness (the stacking axis) and the width of the layer. GSL thus modified becomes orthotropic.

The parameters for orthotropic GSL can be specified using the coordinate system of the tether. The z axis is taken along the stacking direction which is also the thickness direction of the tether. The y and x axes run along the width and length, respectively, of the GSL layer and correspond to the width and length of the tether. For an orthotropic material the response to a force (generalized Hooke's law) can be given by

$$\begin{bmatrix}\epsilon_{xx}\\ \epsilon_{yy}\\ \epsilon_{zz}\\ \epsilon_{yz}\\ \epsilon_{zx}\\ \epsilon_{xy}\end{bmatrix} = \begin{bmatrix} \frac{1}{E_x} & -a_{xy} & -a_{zx} & 0 & 0 & 0\\ -a_{xy} & \frac{1}{E_y} & -a_{yz} & 0 & 0 & 0\\ -a_{zx} & -a_{yz} & \frac{1}{E_z} & 0 & 0 & 0\\ 0 & 0 & 0 & \frac{1}{2G_{yz}} & 0 & 0\\ 0 & 0 & 0 & 0 & \frac{1}{2G_{zx}} & 0\\ 0 & 0 & 0 & 0 & 0 & \frac{1}{2G_{xy}} \end{bmatrix} \begin{bmatrix}\sigma_{xx}\\ \sigma_{yy}\\ \sigma_{zz}\\ \sigma_{yz}\\ \sigma_{zx}\\ \sigma_{xy}\end{bmatrix}, \tag{47}$$

where

$$a_{xy} = \frac{\nu_{xy}}{E_x} = \frac{\nu_{yx}}{E_y}, \qquad a_{zx} = \frac{\nu_{zx}}{E_z} = \frac{\nu_{xz}}{E_x}, \qquad a_{yz} = \frac{\nu_{zy}}{E_z} = \frac{\nu_{yz}}{E_y}.$$

The left-hand column vector contains the normal and shear strains and the right-hand column vector contains the normal and shear stresses. The parameters that must be measured are the Young's moduli, E_x, E_y and E_z, the shear moduli, G_{yz}, G_{zx} and G_{xy}, and the values a_{yz}, a_{zx} and a_{xy} which are the Poisson's ratios ν divided by the Young's moduli.

Electrical conductivity is likely to exhibit anisotropies as well. Each graphene layer within GSL will have a hexagonal array of sp2 electron orbitals above and below its central plane, leading to metal-like conduction in the $x-y$ direction. Perpendicular to the x–y plane, Van der Waals bonds between the layers are unlikely to support a high conductivity. Hence, conductivity in at least two directions will have to be measured.

It is unclear how many heat conductivity parameters will need to be measured. Phonon propagation, important at shorter wavelengths, depends on the molecular structure of GSL and will probably lead to directional heat propagation. In that case, conductivities in the x–y plane and in the z direction will need to be measured. For heat of longer wavelengths, the molecular structure will not be important and one parameter will be sufficient.

The mutual coefficient of friction between the tether material the wheel material will likely be isotropic in the x–y plane of the tether, so only one parameter needs to be measured in this case.

5.2.2. Measurement and testing

Mechanical Properties

For a hypothetical cube of GSL, say 5 cm on a side, obtaining the nine values above would be straightforward: strain gauges on each face would record the responses to tension, compression and shear forces applied by standard testing machines.

An actual sample of tether material, however, would have a thickness of only about 10 μm, with some samples as thin as a few nm. 10 μm samples, which would still have widths and lengths of the order of cm, pose no problem for the above method as long as measurements are restricted to the x–y plane. Strain gauge rosettes applied to this surface could still provide E_x, E_y, G_{xy}, ν_{xy} and ν_{yx} in response to testing machines which grip and pull along the edges of the samples. The remaining parameters, though, could not be obtained in this way because of the small z dimension of the sample.

E_z could be determined by a cantilever bending of the sample in the z direction. The shear moduli could be provided by torsion tests, in which parallel edges of the sample are gripped and twisted along one of the sample's principal axes [52]. The remaining Poisson's ratios could be obtained by measuring the curvatures of micro-machined cantilever plates of GSL [53].

It is difficult or impossible to grip, pull or twist very thin samples without destroying them. Samples would have to be free-standing, mounted or deposited on substrates, or supported in liquid. One method for unsupported thin films could, in principle, measure E_x, E_y, ν_{xy} and ν_{yx} by laser light diffracted from a grating deposited on the sample [54]. Another method uses an ultrasonic micro-spectrometer [55] in which acoustic waves are focused on a sample which is immersed in water. The reflected waves are analyzed to extract the orthotropic parameters.

Using this device, all nine parameters were extracted for a 12 μm thick sample [56].

The nine orthotropic parameters describe only the elastic response of the material. It will also be necessary to measure the full stress–strain curve in order to understand where the elastic region ends and where the yield and breaking points are. Graphene is thought to be near the boundary between a ductile and a brittle material. GSL may or may not have the same behavior.

Electrical and Thermal Properties

Electrical conductivity in the tether is not particularly important at the interface between the climber wheels and the tether material, but it is important in determining the response of the entire space elevator to electromagnetic fields and currents in the atmosphere and space. In this case, the values for in-plane and out-of-plane conductivity are required. Some methods for these measurements are summarized by Rojo et al. [57]. The in-plane measurements involve four probes attached by lithography to the sample at various points. The out-of-plane measurements involve etching the sample, depositing the sample in a mesa-like pattern or placing several probes on the upper surface of the sample and a single large probe on the bottom. The latter method would appear to be most appropriate for GSL.

Values for the in-plane and out-of-plane thermal conductivity are also required. These values are of interest mainly for heat conduction from the wheels into the tether and subsequent dissipation into space. Also, should GSL eventually be used as a radiator material, both in-plane and out-of-plane values will be required for any design. The preferred method for such measurements is transient thermo-reflectance, which depends on the optical reflectance of a material being proportional to the surface temperature of the sample. A variant of this method was carried out for highly oriented pyrolytic graphite [58] which is an in-plane conductor and an out-of-plane insulator. The same test may therefore be appropriate for GSL.

Friction

The coefficient of friction (μ) is a function of the surface conditions of the two materials in contact. The values quoted in this report result from diamond-tipped probes being dragged across samples of graphene, so the value of μ is strictly only valid for diamond on graphene contacts. What is actually needed is the value for the wheel material (titanium) on graphene or GSL. The atomic force microscopes (AFM) used to measure friction on thin samples can be equipped with metal-coated tips [59] so that not only Ti-GSL coefficients, but other metal-GSL coefficients, may be measured. When GSL samples, larger in both thickness and area, are produced, slip testing devices [60] can be used to measure the friction. Here, a sample of one material is dragged across a rigid, fixed plane of another material.

Material Characterization

When GSL is produced it will be necessary to verify that layers of single crystal graphene are being produced and not polycrystalline graphene. The clearest proof of this is the absence of the grain boundaries found in polycrystalline graphene. It will also be essential to demonstrate a low level of defects or impurities in the single crystal graphene planes and in the bonds holding the planes together. These tests can be performed by Raman spectroscopy in which laser light inelastically scattered from a sample provides structural detail of molecules in the material. Raman spectroscopy has already been used for determining grain size, characterizing sp2 and sp3 bonds and determining the number of layers in multi-layer graphene [61]. It should therefore be an ideal tool for the evaluation of the quality of GSL.

5.2.3. Summary of required measurements

Several parameters will need to be measured for GSL before a detailed design of the tether and climber can be made. These are the

elastic response parameters: Young's moduli along principal material axes E_x, E_y, E_z, shear moduli G_{xy}, G_{yz}, G_{xz} and the Poisson's ratios ν_{xy}, ν_{yz}, ν_{xz},

stress–strain curves from zero to breaking stress for tension, σ_{BS}, shear, τ_{BS} and compression,

electrical conductivity in-plane κ_{xy} and out-of-plane κ_z,

thermal conductivity in-plane λ_{xy} and out-of-plane λ_z,

coefficient of friction μ with metals, especially titanium and

material characterization: absence of grain boundaries, absence of defects and number of layers.

5.3. Tether design and trade study

The optimal set of material parameters for the tether will result from a study in which parameters of the multi-dimensional design space are traded against one another to achieve maximum performance. Numerous trades of tether material parameters and conditions are defined here. In addition, there are different tether configurations which may be used.

Material trades involve a large number of parameters. For each possible tether material, CNTs, GSL or hBN, the following trade spaces must be examined: strength vs. flexibility, stiffness vs. rigidity, electrical conductivity vs. time, tensile strength vs. load vs. time, fracture rate vs. time, friction vs. load and yield strength vs. load vs. time.

Configuration trades deal with how the tether is physically arranged and what loads it will bear. An actual space elevator may employ one or more tethers and each tether may have a curved or flat profile, for example. A tether may be composed of a varying number of molecular layers and the best number will result from a trade of the resulting total mass vs. strength. The three-dimensional trade space of maximum stress, load and length will have to be explored as will the space defined by maximum pressure, load and length.

Trades having to do with the climber–tether interface include climb duration vs. altitude in vacuum and in atmosphere, friction force vs. load vs. time, temperature vs. location vs. time, minimum and maximum stress vs. load vs. time, contact length of wheels on the tether vs. Young modulus vs. Poisson's Ratio vs. stress vs. motor torque and temperature vs. expansion.

6. Conclusions

The conditions at the climber–tether interface, established in Section 2, set physical requirements for the space elevator tether, a wheeled climber and the region where they make contact. Design considerations for both the climber and tether indicated the need for future developments. The state of the art in strong materials production has advanced rapidly in recent years. It is likely that materials satisfying the requirements of a space elevator tether will become available in the near future. The requirements, as established by the climbability conditions, are listed here.

The coefficient of friction of GSL must be increased. The coefficient friction for graphene and therefore GSL is between 0.03 and 0.1. In order to increase the efficiency of a gripping wheel drive, this must be increased. Two methods were proposed which could double this value: adsorbing hydrogen onto the surface and using hexagonal boron nitride bonded to the outer graphene layers.

The shear strength of GSL must be increased. While the tensile strength of GSL is sufficient to support the mass of a tether and its climbers, its shear strength is not. The shear may be increased by the cross-bonding

the graphene layers using high pressure to convert some of its carbon sp2 bonds to the "diamond" sp3 bond.

Orthotropic material properties of strong materials must be measured. GSL is likely to be an orthotropic material, so its nine elastic response parameters must be measured. Anisotropies in the electrical and thermal properties of GSL also need to be measured. The same may well be required for other strong materials.

Testing of materials under interface conditions must be done. Tests specially devised for multi-layer two-dimensional materials must be performed. These include quality control issues such as the absence of domain boundaries, defects in the crystal lattice and intercalated gasses. Response to heat, cold and total combined stress must also be tested.

Molecular modeling is needed. Whether the above two proposals will work must of course be tested in the laboratory. Before that, however, molecular modeling of layered 2D materials could guide improvements to the improved material production process.

More research is required into production of high-strength materials. The key to the construction of the space elevator is the availability of a large amount of strong materials of sufficient length. Many methods of fast production are now being developed, but to date, none have achieved the length or rate required. At this time, there are no known physical limitations to large increases in the GSL production rate, so the outlook remains optimistic.

Declaration of competing interest

The authors declare that they have no known competing financial interests or personal relationships that could have appeared to influence the work reported in this paper.

Appendix. Material properties

Material properties are presented for graphene super-laminate (GSL), hexagonal boron nitride (hBN) and single-walled carbon nanotubes (SWCNT).

A.1. Mechanical properties

The following abbreviations are used in Table A.1:

ρ	Mass density (kg/m^3)
σ_{TS}	Ultimate tensile strength (GPa)
τ_{SS}	Shear strength (GPa)
E	Young's modulus (GPa)
G	Shear modulus (GPa)
σ_{BS}	Breaking strength (N/m)
E_{2D}	Second order elastic stiffness (N/m)
D_{2D}	Third order elastic stiffness (N/m)
μ	Coefficient of friction

A.2. Electrical, thermal and optical properties

The following abbreviations are used in Table A.2:

κ	Electrical conductivity (S/m)
j_{BD}	Breakdown current density (A/m^2)
M.P.	Melting point (K)
c_g	Specific heat capacity at 300 K (J/kg/K)
λ	In-plane thermal conductivity (W/m/K)
α	Visible light absorptivity (%)

Table A.1
Mechanical properties of possible tether materials.

Measure	GSL	hBN	SWCNT
ρ	2298	2200 [62]	1600 [63]
σ_{TS}	70–130 [20]	100.5 [28]	77–200 [64]
τ_{SS}	0.14 [22]	3.07–4.31 [27]	
E	1000 [20]	716–977 [65]	1000 [64]
G	0.19–0.49 [27]	3.07–4.31 [27]	470 [66]
σ_{BS}	42 [20]	23.6 ± 1.8 [65]	44–174 [67]
E_{2D}	350 ± 50 [20]	290 ± 24 [65]	[a]
D_{2D}	−650 ± 120 [20]	−680 [65]	[a]
μ	0.03 [41]–0.10 [26]	0.23–0.27 [31]	0.22–0.24 [68]

[a]Not applicable to 1D materials.

Table A.2
Electrical, thermal and optical properties of possible tether materials.

Measure	SCG	hBN	SWCNT
κ	9.6×10^7 [24]	1.89×10^{-7} [69]	7.3×10^4 [70]
j_{BD}	10^{12} [71]	5000 [72]	10^7–10^9 [73]
M.P.	5000–6000 [74]	2900 [62]	4800 [75]
c_g	706.9 [76]	874 [77]	650 [78]
λ	5000 [24]	751 [30]	6600 [79]
α	2.3 [24]	0 [80]	

References

[1] B. Shelef, The space elevator feasibility condition, Climb 1 (2011) 85–92.
[2] B.C. Edwards, E.A. Wesling, The Space Elevator: A Revolutionary Earth-To-Space Transportation System, BC Edwards, Houston, 2002.
[3] X. Xu, Z. Zhang, J. Dong, D. Yi, J. Niu, M. Wu, L. Lin, R. Yin, M. Li, J. Zhou, S. Wang, J. Sun, X. Duan, P. Gao, Y. Jiang, X. Wu, H. Peng, R.S. Ruoff, Z. Liu, D. Yu, E. Wang, F. Ding, K. Liu, Ultrafast epitaxial growth of metre sized single-crystal graphene on industrial cu foil, Sci. Bull. 62 (2017) 1074–1080.
[4] L. Wang, X. Xu, L. Zhang, R. Qiao, M. Wu, Z. Wang, S. Zhang, J. Liang, Z. Zhang, Z. Zhang, W. Chen, X. Xie, J. Zong, Y. Shan, Y. Guo, M. Willinger, H. Wu, Q. Li, W. Wang, P. Gao, S. Wu, Y. Zhang, Y. Jiang, D. Yu, E. Wang, X. Bai, Z.-J. Wang, F. Ding, K. Liu, Epitaxial growth of a 100-square centimetre single-crystal hexagonal boron nitride monolayer on copper, Nature 570 (2019) 91–95.
[5] R. Zhang, Y. Zhang, Q. Zhang, H. Xie, W. Qian, F. Wei, Growth of half-meter long carbon nanotubes based on schulz–flory distribution, ACS Nano 7 (2013) 6156–6161.
[6] A. Nixon, R. Whieldon, D. Nelson, Graphene: Manufacturing, Applications and Economic Impact, Nixene Publishing, Manchester, UK, 2021.
[7] P.A. Swan, D.L. Raitt, C.W. Swan, R.E. Penny, J.K. Knapman, Space Elevators: An Assessment of the Technological Feasibility and the Way Forward, Virginia Edition Publishing Company, Houston, USA, 2013.
[8] D.H. Wright, L. Bartoszek, A. Burke, D. Dotson, H. El-Chab, J. Knapman, M. Lades, A. Nixon, J. Paul W. Phister, P. Robinson, The Climber-Tether Interface of the Space Elevator, Tech. rep., International Space Elevator Consortium, 2023, Accessed: 6 April 2023.
[9] MaterialProperties, Graphite: Density, strength, hardness, melting point, 2022, Accessed: 14 August 2022.
[10] P.A. Swan, C.W. Swan, R.E. Penny, J.M. Knapman, P.N. Glaskowsky, Design Considerations for Space Elevator Tether Climbers, Tech. rep., International Space Elevator Consortium, 2013.
[11] S. Cohen, A.K. Misra, Static deformation of space elevator tether due to climber, Acta Astronaut. 111 (2015) 317–322.
[12] maglev.net, All you need to know about the world's fastest train, 2018, Accessed 13 June 2023.
[13] M. Today, Terrier armored engineer vehicle, 2023, Accessed 13 June 2023.
[14] P. Robinson, Space elevator climber dynamics and climb frequency optimisation, Acta Astronaut. 210 (2023) 518–528.
[15] HelixMotor, Space elevator climber dynamics and climb frequency optimisation, 2022, Accessed 26 October 2022.
[16] J. Shigley, C. Mischke, Mechanical Engineering Design, 5th Edition, McGraw-Hill, Inc., New York, 1989.
[17] A. Aerospace Specification Metals Inc., Titanium ti-6al-4V (grade 5), annealed, 2022, Accessed: 15 April 2022.
[18] M. Janecek, F. Novy, P. Harcuba, J. Strasky, L. Trsko, M. Mhaede, L. Wagner, The very high cycle fatigue behaviour of ti-6al-4V alloy, Acta Phys. Polon. A 128 (2015) 497–502.
[19] J.J. Zipay, T.C. Modlin, C.E. Larsen, The Ultimate Factor of Safety for Aircraft and Spacecraft – Its History, Applications and Misconceptions, Tech. rep., NASA, 2015, NASA Doc. ID 20150003482.

[20] C. Lee, X. Wei, J.W. Kysar, J. Hone, Measurement of the elastic properties and intrinsic strength of monolayer graphene, Science 321 (2008) 385–388.
[21] A. Yoshiasa, Y. Murai, O. Ohtaka, T. Katsura, Detailed structures of hexagonal diamond (lonsdaleite) and wurtzite-type BN, Japan. J. Appl. Phys. 42 (2003) 1694.
[22] Z. Liu, S.-M. Zhang, J.-R. Yang, J.Z. Liu, Y.-L. Yang, Q.-S. Zheng, Interlayer shear strength of single crystalline graphite, Acta Mech. Sinica 28 (2012) 978–982.
[23] D.H. Wright, L. Bartoszek, D. Dotson, D. Gleeson, J. Knapman, M. Lades, A. Nixon, P. Phister, P. Robinson, The climber-tether interface of the space elevator, 2021, Presented at 72nd International Astronautical Conference, Dubai.
[24] C. for Physics of the Royal Swedish Academy of Sciences, Graphene - scientific background on the nobel prize in physics 2010, 2010, Accessed: 14 August 2022.
[25] T. Latychevskaia, S.-K. Son, Y. Yang, D. Chancellor, M.L. Brown, S. Ozdemir, I. Madan, G. Berruto, F. Carbone, A. Mishchenko, K.S. Novoselov, Stacking transition in rhombohedral graphite, Front. Phys. 14 (2019) 13608.
[26] N. Dwivedi, A.K. Ott, K. Sasikumar, C. Dou, R. Yeo, B. Narayanan, U. Sassi, D.D. Fazio, G. Soavi, T. Dutta, O. Balci, S. Shinde, J. Zhang, A. Katiyar, P. Keatley, A. Srivastava, S. Sankaranarayanan, A.C. Ferrari, C. Bhatia, Graphene overcoats for ultra-high storage density magnetic media, Nature Commun. 12 (2021) 2854.
[27] W. Qu, S. Bagchi, X. Chen, H.B. Chew, C. Ke, Bending and interlayer shear moduli of ultrathin boron nitride nanosheet, J. Phys. D: Appl. Phys. 52 (2019) 465301.
[28] R. Paul, T. Tasnim, R. Dhar, S. Mojumder, S. Saha, M.A. Motalab, Study of uniaxial tensile properties of hexagonal boron nitride nanoribbons, 2017, Accessed: 20 February 2021.
[29] A. Lipp, K.A. Schwetz, K. Hunold, Hexagonal boron nitride: Fabrication, properties and applications, J. Eur. Ceram. Soc. 5 (1989).
[30] Q. Cai, D. Scullion, W. Gan, A. Falin, S. Zhang, K. Watanabe, T. Taniguchi, Y. Chen, E. Santos, L.H. Li, High thermal conductivity of high-quality monolayer boron nitride and its thermal expansion, Sci. Adv. 5 (6) (2019).
[31] J.O. Koskilinna, M. Linnolahti, T.A. Pakkanen, Friction coefficient for hexagonal boron nitride surfaces from ab initio calculations, Tribol. Lett. 24 (2006) 37–41.
[32] Tuball, About tuball, 2022, Accessed: 16 August 2022.
[33] H. Sugime, T. Sato, R. Nakagawa, T. Hayashi, Y. Inoue, S. Noda, Ultra-long carbon nanotube forest via in situ supplements of iron and aluminum vapor sources, Carbon 172 (2021) 772–780.
[34] Grolltex, Boron nitride manufacturer grolltex; graphene rolling technologies, 2022, Accessed: 16 August 2022.
[35] A. Nixon, Forward thinking about the CVD graphene market, Nixene J. 6 (2022) 8–11.
[36] A. Nixon, Charmgraphene: development of graphene-based pellicle for EUV, Nixene J. 5 (2021) 43.
[37] I. Vlassiouk, Y. Stehle, P. Pudasaini, R. Unocic, P. Rack, A. Baddorf, I. Ivanov, N. Lavrik, F. List, N. Gupta, K. Bets, B. Yakobson, S. Smirnov, Evolutionary selection growth of two-dimensional materials on polycrystalline substrates, Nature Mater. 17 (2018) 318–322.
[38] Y. Ishikawa, Y. Fuchita, T. Hitomi, Y. Inoue, M. Karita, K. Hayashi, T. Nakano, N. Baba, Survivability of carbon nanotubes in space, Acta Astronaut. 165 (2019) 129.
[39] F.C. Maia, R.E. Samad, J. Bettini, R.O. Freitas, J. Nilson D. Vieira, N.M. Souza-Neto, Synthesis of diamond-like phase from graphite by ultrafast laser driven dynamical compression, Sci. Rep. 5 (2015) 11812.
[40] C. Niu, J. Zhang, H. Zhang, J. Zhao, W. Xia, Z. Zeng, X. Wang, Configuration stability and electronic properties of diamane with boron and nitrogen dopants, Phys. Rev. B 105 (2022) 174106.
[41] Y.J. Shin, R. Stromberg, R. Nay, H. Huang, A.T.S. Wee, H. Yang, C.S. Bhatia, Frictional characteristics of exfoliated and epitaxial graphene, 2011, Accessed: 18 February 2021.
[42] L.-F. Wang, T.-B. Ma, Y. Hu, H. Wang, T.-M. Shao, Ab initio study of the friction mechanism of fluorographene and graphene, J. Chem. C 117 (2013) 12520–12525.
[43] M. Yankowitz, Q. Ma, P. Jarillo-Herrero, B.J. LeRoy, Van der waals heterostructures combining graphene and hexagonal boron nitride, Nat. Rev. Phys. 1 (2019) 112–125.
[44] SAMSON, SAMSON: platform for integrated molecular design, 2022, Accessed: 15 September 2022.
[45] LAMMPS, LAMMPS molecular dynamics simulator, 2022, Accessed: 15 September 2022.
[46] GROMACS, GROMACS: Software suite for high-performance molecular dynamics, 2022, Accessed: 15 September 2022.
[47] VASP, VASP: The vienna ab initio simulation package, 2022, Accessed: 15 September 2022.
[48] D.W. Brenner, O.A. Shenderova, J.A. Harrison, S.J. Stuart, B. Ni, S.B. Sinnott, A second-generation reactive empirical bond order (REBO) potential energy expression for hydrocarbons, J. Phys.: Condens. Matter 14 (2002) 783.
[49] R.C. Sinclair, J.L. Suter, P.V. Coveney, Graphene–graphene interactions: Friction, superlubricity, and exfoliation, Adv. Mater. Commun. 30 (2018) 1705791.
[50] P. Hohenberg, W. Kohn, Inhomogeneous electron gas, Phys. Rev. 136 (1964) B864–B871.
[51] L.J. Gibson, M.F. Ashby, Cellular Solids: Structure and Properties, Cambridge University Press, Cambridge, UK, 1997.
[52] B.M. Lempriere, R.W. Fenn, D.D. Crooks, W.C. Kinder, Torsion testing for shear modulus of thin orthotropic sheet, AIAA J. 7 (1969) 2341–2342.
[53] P. Krulevitch, A technique for determining the Poisson's ratio of thin films (UCRL-JC-123344; CONF-961105-3), Tech. rep., Lawrence Livermore National Lab, 1996.
[54] J.A. Ruud, D. Josell, F. Spaepen, A.L. Greer, A new method for tensile testing of thin films, J. Mater. Res. 8 (1993) 112–117.
[55] Y. Tsukahara, K. Ohira, N. Nakaso, An ultrasonic micro-spectrometer for the evaluation of elastic properties with microscopic resolution, 1990, Presented at IEEE Symposium on Ultrasonics, https://ieeexplore.ieee.org/document/171498.
[56] Y. Okabe, N. Takeda, M. Yanaka, Y. Tsukahara, Determination of the orthotropic elastic constants of thin PET film by an ultrasonic micro-spectrometer, IEEE Trans. Ultrason. Ferroelectr. Freq. Control 46 (1999) 1269–1275.
[57] M.M. Rojo, C.V. Manzano, D. Granados, M.R. Osorio, T. Borca-Tasciuc, M. Martin-Gonzalez, High electrical conductivity in out of plane direction of electrodeposited Bi2Te3 films, AIP Adv. 5 (2015) 087142.
[58] D. Rodin, S.K. Yee, Simultaneous measurement of in-plane and through-plane thermal conductivity using beam-offset frequency domain thermoreflectance, Rev. Sci. Instrum. 88 (2017) 014902.
[59] K. Xu, Y. Liu, Studies of probe tip materials by atomic force microscopy: a review, Beilstein J. Nanotechnol. 13 (2022) 1256–1267.
[60] Y. Gao, Friction and peel tester thin film test, 2015, Accessed: 3 November 2022.
[61] A.R. Barron, Nanomaterials and Nanotechnology, openstax.org Rice University, Houston, 2015.
[62] S. Roy, X. Zhang, A.B. Puthirath, A. Meiyazhagan, S. Bhattacharyya, M.M. Rahman, G. Babu, S. Susarla, S.K. Saju, M.K. Tran, L.M. Sassi, M.A.S.R. Saadi, J. Lai, O. Sahin, S.M. Sajadi, B. Dharmarajan, D. Salpekar, N. Chakingal, A. Baburaj, X. Shuai, A. Adumbumkulath, K.A. Miller, J.M. Gayle, A. Ajnsztajn, T. Prasankumar, V.V.J. Harikrishnan, V. Ojha, H. Kannan, A.Z. Khater, Z. Zhu, S.A. Iyengar, P.A. da Silva Autreto, E.F. Oliveira, G. Gao, A.G. Birdwell, M.R. Neupane, T.G. Ivanov, J. Taha-Tijerina, R.M. Yadav, S. Arepalli, R. Vajtai, P.M. Ajayan, Structure, properties and applications of two-dimensional hexagonal boron nitride, Adv. Mater. 33 (2021) 2101589.
[63] H. Sugime, S. Esconjauregui, J. Yang, L. D'Arsié, R. Oliver, S. Bhardwaj, C. Cepek, J. Robertson, Low temperature growth of ultra-high mass density carbon nanotube forests on conductive supports, Appl. Phys. Lett. 103 (2013) 073116.
[64] A. Takakura, K. Beppu, T. Nishihara, A. Fukui, T. Kozeki, T. Namazu, Y. Miyauchi, K. Itami, Strength of carbon nanotubes depends on their chemical structures, Nature Commun. 10 (2019) 3040.
[65] A. Falin, Q. Cai, E.J. Santos, D. Scullion, D. Qian, R. Zhang, Z. Yang, S. Huang, K. Watanabe, T. Taniguchi, M.R. Barnett, Y. Chen, R.S. Ruoff, L.H. Li, Mechanical properties of atomically thin boron nitride and the role of interlayer interactions, Nature Commun. (2017) 15815.
[66] C.W. To, Bending and shear moduli of single-walled carbon nanotubes, Finite Elem. Anal. Des. 42 (2006) 404–413.
[67] M.-F. Yu, B.S. Files, S. Arepalli, R.S. Ruoff, Tensile loading of ropes of single wall carbon nanotubes ands their mechanical properties, Phys. Rev. Lett. 84 (2000) 5552.
[68] G. Yamamoto, T. Hashida, K. Adachi, T. Tagaki, Tribological properties of single-walled carbon nanotube solids, J. Nanosci. Nanotechnol. 8 (2008) 2665–2670.
[69] S. Deng, Y. Gu, X. Wan, M. Gao, S. Xu, K. Chen, H. Chen, Probing electronic properties of CVD monolayer hexagonal boron nitride by an atomic force microscope, Front. Mater. 8 (2021) This paper gives the electrical resistivity for monolayer CVD hBN as 529 MΩ/cm. This was converted to S/m using the converter at https://www.cactus2000.de/uk/unit/masscnd.php.
[70] I. Puchades, C.C. Lawlor, C.M. Schauerman, A.R. Bucossi, J.E. Rossi, N.D. Coxa, B.J. Landi, Mechanism of chemical doping in electronic-type-separated single wall carbon nanotubes towards high electrical conductivity, J. Mater. Chem. C 3 (2015) 10256–10266.
[71] R. Murali, Y. Yang, K. Brenner, T. Beck, J.D. Meindl, Breakdown current density of graphene nanoribbons, Appl. Phys. Lett. 94 (2009) 243114.
[72] A. Pierret, D. Mele, H. Graef, J. Palomo, T. Taniguchi, K. Watanabe, Y. Li, B. Toury, C. Journet, P. Steyer, V. Garnier, A. Loiseau, J.-M. Berroir, E. Bocquillon, G. Feve, C. Voisin, E. Baudin, M. Rosticher, B. Placais, Dielectric permittivity, conductivity and breakdown field of hexagonal boron nitride, Mater. Res. Express 9 (2022) 065901.
[73] X. Wang, N. Behabtu, C.C. Young, D.E. Tsentalovich, M. Pasquali, J. Kono, High ampacity power cables of tightly-packed and aligned carbon nanotubes, Adv. Funct. Mater. 24 (2014) 3241–3249.
[74] E. Ganz, A.B. Ganz, L.-M. Yang, M. Dornfeld, The initial stages of melting of graphene between 4000 k and 6000 k, Phys. Chem. Chem. Phys. 19 (2017) 3756–3762.
[75] K. Zhang, G.M. Stocks, J. Zhong, Melting and premelting of carbon nanotubes, Nanotechnology 18 (2007) 285703.
[76] S. Picard, D.T. Burns, P. Roger, Determination of the specific heat capacity of a graphite sample using absolute and differential methods, Metrologia 44 (2007) 294.

[77] S.K. Singh, M. Neek-Amal, S. Costamagna, F.M. Peeters, Thermomechanical properties of a single hexagonal boron nitride sheet, Phys. Rev. B 87 (2013) 184106.
[78] J. Hone, A.T. Johnson, Z. Benes, J.E. Fischer, Quantized phonon spectrum of single-wall carbon nanotubes, Science 289 (2000) 1730–1733.
[79] S. Berber, Y.-K. Kwon, D. Tomanek, Unusually high thermal conductivity of carbon nanotubes, Phys. Rev. Lett. 84 (2000) 4613–4616.
[80] J. Wang, F. Ma, M. Sun, Graphene, hexagonal boron nitride and their heterostructures: properties and applications, R. Soc. Chem. Adv. 7 (2017) 16801–16822.